

1 **Title: Rapid evolution of bacterial mutualism in the plant rhizosphere**

2

3 **Authors/ Affiliations**

4 Erqin Li^{1,2,3}, Ronnie de Jonge^{1,4,5*}, Chen Liu¹, Henan Jiang¹, Ville-Petri Friman⁶, Corné M.J.
5 Pieterse¹, Peter A.H.M. Bakker^{1*} and Alexandre Jousset^{7*}

6 ¹Utrecht University, Department of Biology, Plant-Microbe Interactions, Padualaan 8, 3584 CH,
7 Utrecht, The Netherlands.

8 ²Freie Universität Berlin, Institut für Biologie, Altensteinstr. 6, D-14195 Berlin, Germany.

9 ³Berlin-Brandenburg Institute of Advanced Biodiversity Research, D-14195 Berlin, Germany.

10 ⁴VIB Center for Plant Systems Biology, Technologiepark 952, B-9052, Ghent, Belgium.

11 ⁵Ghent University, Department of Plant Biotechnology and Bioinformatics, Technologiepark 952,
12 B-9052, Ghent, Belgium.

13 ⁶University of York, Department of Biology, Wentworth Way, YO10 5DD, York, United
14 Kingdom.

15 ⁷Utrecht University, Department of Biology, Ecology and Biodiversity, Padualaan 8, 3584 CH,
16 Utrecht, The Netherlands.

17 **Author List Footnotes**

18 Further information and requests for resources and reagents should be directed to and will be
19 fulfilled by the Lead Contact, Alexandre Jousset (A.L.C.Jousset@uu.nl).

20 *Correspondence to: A.L.C.Jousset@uu.nl, P.A.H.M.Bakker@uu.nl, r.dejonge@uu.nl

21

22 **Summary**

23 Even though beneficial plant-microbe interactions are commonly observed in nature, direct
24 evidence for the evolution of bacterial mutualism in the rhizosphere remains elusive. Here we use
25 experimental evolution to causally show that initially plant-antagonistic *Pseudomonas protegens*
26 bacterium evolves into mutualists in the rhizosphere of *Arabidopsis thaliana* within six plant
27 growth cycles (6 months). This evolutionary transition was accompanied with increased mutualist
28 fitness via two mechanisms: *i*) improved competitiveness for root exudates and *ii*) enhanced
29 capacity for activating the root-specific transcription factor gene *MYB72*, which triggers the
30 production of plant-secreted scopoletin antimicrobial for which the mutualists evolved relatively
31 higher tolerance to. Genetically, mutualism was predominantly associated with different mutations
32 in the GacS/GacA two-component regulator system, which conferred high fitness benefits only in
33 the presence of plants. Together, our results show that bacteria can rapidly evolve along the
34 parasitism-mutualism continuum in the plant rhizosphere at an agriculturally relevant evolutionary
35 timescale.

36 **Keywords:** experimental evolution, mutualism, plant-microbe interaction, diversification,
37 rhizosphere, genetics

38

39 **Introduction**

40 Mutualistic interactions between multicellular hosts and their associated microbiota are important
41 for the fitness of both parties ¹⁻⁴. However, while commonly observed in nature, direct evidence
42 for the evolution of mutualism at both phenotypic and genotypic level is still scarce ⁵⁻⁷. The
43 rhizosphere is a hotspot for mutualistic interactions between the plant and free-living
44 microorganisms. For example, plants can preferentially interact with mutualistic microbes present
45 in the indigenous species pool of the soil and disproportionately increase their relative abundances
46 in the rhizosphere ⁸⁻¹⁰. While such plant-mediated ecological filtering can rapidly change the
47 relative abundances of mutualistic versus antagonistic species in the rhizosphere, it is less clear if
48 plants can drive evolution of mutualism within species by increasing the fitness of emerging *de*
49 *novo* mutualist genotypes. For example, even the most well-known plant mutualistic microbes,
50 nitrogen-fixing rhizobia ⁵ and phosphorus-providing mycorrhizae ¹¹, can be detrimental to the
51 plant, suggesting that the interaction between a given pair of plant and microorganism varies
52 naturally ^{12,13}. It is thus possible that plant-associated microbes might evolve along the parasitism-
53 mutualism continuum in response to selection exerted by plants.

54 Beneficial symbioses between eukaryotic and prokaryotic organisms have evolved multiple
55 times across the eukaryotic domain ¹⁴ and are considered as one of the major evolutionary
56 transitions of life ¹⁵. It has been suggested that the evolution of mutualism often requires two basic
57 components: currency and mechanism of exchange of the currency ¹⁴. In the context of plant-
58 bacteria interactions, currency could be, for example, a root exudate, which can be taken up by
59 bacteria. Similarly, bacteria might produce plant growth-promoting hormones such as auxin and
60 gibberellins ¹⁶, that are beneficial for plant growth. When the currency exchange between both
61 parties is symmetrical, the selection is expected to favour the evolution of mutualism. Increased

62 mutualistic dependence is then thought to evolve via reciprocal coevolution or via adaptation by
63 one of the partners via selection on traits that are directly involved in the mutualistic interaction ¹⁵.
64 However, currency exchange could also be asymmetrical, due to competition for shared limiting
65 nutrients, such as iron ¹⁷, which could explain why certain plant-microbe interactions are
66 antagonistic. Moreover, due to the open nature of the rhizosphere, free diffusion of plant-derived
67 resources could select for increased levels of cheating where mutant bacterial genotypes take
68 advantage of ‘public goods’ without contributing to the production of plant growth-promoting
69 compounds ^{5,17}. As a result, mutualistic plant-microbe interactions might require additional
70 enforcing from the plant ⁵ via sanctioning of cheating bacterial genotypes.

71 To assess whether plant-microbe mutualism can emerge as a consequence of plant-
72 mediated effects, we used an *in vivo* experimental evolution design ¹⁸ where we allowed the
73 rhizosphere bacterium *Pseudomonas protegens* CHA0 to evolve on the roots of *Arabidopsis*
74 *thaliana* in the absence of other microbes. Furthermore, we used sterile sand free of organic carbon
75 as the growth substrate making bacterial growth obligately dependent on plant root exudates. As a
76 result, bacterial survival and evolution was solely dependent on the presence of the plant, and the
77 performance of evolved bacterial selection lines were thus compared with the ancestral bacterial
78 strain. To set up the selection experiment, we inoculated a clonal bacterial population on the roots
79 of five independent *A. thaliana* Col-0 replicate plant selection lines and grew the plants and *P.*
80 *protegens* in otherwise gnotobiotic conditions for a total of six plant growth cycles, which lasted
81 four weeks each. At the end of every growth cycle, the evolved bacterial populations were isolated
82 and transferred to the rhizosphere of new sterile plants (Fig. S1). In these experimental conditions,
83 the initial plant-bacterium interaction was antagonistic: *A. thaliana* aboveground biomass was
84 clearly reduced in the presence of *P. protegens* CHA0 after one growth cycle ($F_{1,8} = 45.4$, $P <$
85 0.001 , Fig. 1A), and likely cause for this is the production of diverse bioactive metabolites by

86 CHA0¹⁹ that can constrain plant growth²⁰. To quantify changes in plant-bacterium interaction,
87 sixteen evolved bacterial colonies were randomly selected from each plant replicate selection line
88 at the end of the second, fourth and sixth growth cycles, in addition to sixteen randomly selected
89 ancestral colonies (in total 256 isolates). Each isolated colony was characterized phenotypically by
90 measuring multiple key life-history traits, including growth on different carbon sources and media,
91 tolerance to diverse abiotic and biotic stresses, production of several bioactive compounds and their
92 ability to inhibit other microorganisms (Table S1). A subset of bacterial phenotypes was also full
93 genome sequenced and characterised for their effects on plant growth in terms of root architecture
94 and above and belowground biomasses at the end of the selection experiment.

95 **Results**

96 *Selection in the plant rhizosphere leads to bacterial phenotypic diversification and evolutionary* 97 *transition towards mutualism*

98 To study the evolution of *P. protegens* CHA0 in the *A. thaliana* rhizosphere, we isolated a total of
99 240 evolved bacterial isolates from every second time point along with sixteen ancestral isolates
100 (Supplementary dataset 1) and used K-means clustering analysis to separate them into five distinct
101 phenotypic groups based on measured all life-history traits (Fig. S2, Table S2). The phenotypic
102 groups were then given names that reflected key differences in their appearance, life-history traits,
103 and their mean effects on plant growth (Fig. 1; Fig. S3-S4). Evolved clones that clustered together
104 with the ancestral strain were named as ‘Ancestral-like’ phenotype. Another phenotype similar to
105 the ancestral strain, which only appeared momentarily before dropping below detection level was
106 named as ‘Transient’ phenotype (Figs. 1-2). A third phenotype that resembled the ancestral strain,
107 but which had clearly reduced abiotic stress tolerance ($F_{5, 248} = 40.8$, $P < 0.001$, Fig. S4) and
108 increased ability to form a biofilm ($F_{5, 249} = 196.8$, $P < 0.001$, Fig. S4), was named as ‘Stress-

109 sensitive' phenotype. Agar plate assays were used to determine the effect of the evolved
110 phenotypes on *A. thaliana* growth. While the 'Ancestral-like', 'Transient' and 'Stress-sensitive'
111 phenotypes showed neutral effects on plant biomass relative to plant-only control lines (Shoot
112 biomass, $F_{6,26} = 8.01$, $P < 0.001$; Root biomass, $F_{6,26} = 2.84$, $P = 0.029$, Fig. 1), they had a negative
113 effect on the plant root length (Root length, $F_{6,26} = 10.01$, $P < 0.001$, Fig. 1E) and resulted in clear
114 bleaching of plants indicative of reduced chlorophyll activity similar to the ancestor (the amount
115 of green pixels, $F_{6,26} = 5.90$, $P < 0.001$, Fig. 1F). These assays also revealed two novel phenotypes
116 that showed positive effects on plant shoot and root biomasses (Fig. 1B, C) with comparable levels
117 of plant 'greenness' to no-bacteria control treatment (Fig. 1F). These evolved phenotypes were
118 therefore named as 'Mutualist 1' and 'Mutualist 2' as indicated by their plant growth-promoting
119 activity.

120 The relative abundance of different phenotype groups changed over time (Fig. 2A). The
121 'Ancestral-like' phenotypes persisted throughout the experiment even though they were substituted
122 by evolved phenotypes in all plant selection lines (Fig. 2A). The evolutionary success of 'Transient'
123 and 'Stress-sensitive' phenotypes was short-lived: 'Transient' phenotypes disappeared below the
124 detection limit in all plant selection lines by the end of the sixth growth cycle (Fig. 2A), while the
125 'Stress-sensitive' phenotypes emerged only in three selection lines and survived until the end of
126 the experiment only in one of the selection lines (Fig. 2A). In contrast, the frequency of mutualistic
127 phenotypes increased in four out of five plant selection lines throughout the experiment, while one
128 selection line became dominated by 'Ancestral-like' and 'Stress-sensitive' phenotypes (Fig. 2A).

129 An aggregated 'plant performance' index summarising the effects of each bacterial isolate
130 on both aboveground and belowground plant growth traits (Fig. 2B, PC1 of multivariate analysis),
131 was used to explore if reduced antagonism towards the plant was associated with improved
132 bacterial growth indicative of the evolution of reciprocally beneficial mutualistic interaction. We

133 found a significant positive correlation between plant performance index and bacterial phenotype
134 abundance per plant ($F_{1, 28} = 8.01$, $P < 0.001$, Fig. 2C). Specifically, both mutualistic phenotypes
135 reached higher abundances in the plant rhizosphere compared to other phenotypes (bacterial cells
136 per plant). This indicates that reduced bacterial antagonism towards the plant was coupled with
137 improved growth in the rhizosphere, which could also explain why mutualists became the dominant
138 phenotypes in four out of five plant selection lines during the selection experiment (reaching up to
139 94% relative abundance, Fig. 2A). In support for this, a similar positive correlation was observed
140 between the degree of plant performance of each phenotype measured in separate plant growth
141 assays and their relative abundance in diversified rhizosphere populations at the end of the selection
142 experiment ($F_{1, 23} = 4.37$, $P = 0.048$, Fig. S5). Together, these results demonstrate that the evolution
143 of plant-growth promotion was accompanied with increased bacterial fitness, indicative of a
144 mutualistic interaction where each species had a net benefit. As this evolutionary transition was
145 observed parallel in four out of five selection lines, it was likely driven by deterministic processes
146 such as selection exerted by the plant instead of random genetic drift due to bottlenecks between
147 plant growth cycles.

148
149 ***Evolution of mutualism is linked to improved resource catabolism and tolerance to plant-***
150 ***secreted antimicrobials***

151 For stable mutualism to evolve, plants would need to provide the evolved mutualists a ‘currency’
152 that could not be accessed by the other phenotypes or employ some form of ‘sanctioning’ to
153 constrain the growth of non-mutualist phenotypes. To study this, we first compared differences in
154 the evolved phenotypes’ ability to use a range of carbon sources that are typically found in *A.*
155 *thaliana* root exudates²¹, and which could have selectively preferred the growth of mutualist
156 phenotypes. Second, we compared the evolved phenotypes’ tolerance to scopoletin, which is an

157 antimicrobial secreted by plant roots known to modulate root microbiome composition for example
158 by favouring more tolerant bacterial taxa^{22,23}. We found that the ‘Mutualist 1’ phenotype showed
159 an improved ability to grow on various different carbon sources compared to the other phenotypes
160 (PC1 of multivariate analysis, $F_{5,248} = 50.72$, $P < 0.001$, Fig. 3A). This suggests that ‘Mutualist 1’
161 potentially evolved an ability to compete better for plant-derived root exudates during the selection
162 experiment, which could have increased their abundance relative to other phenotypes. Moreover,
163 ‘Transient’, ‘Stress-sensitive’ and ‘Mutualist 2’ phenotypes showed reduced growth on carbon
164 sources relative to ‘ancestral-like’ phenotypes indicative of competitive disadvantage (Fig. 3A).
165 To explore the potential significance of scopoletin, we used a GUS reporter assay to determine how
166 different bacterial phenotypes affected the expression of the plant root-specific gene *MYB72*²⁴,
167 which encodes a transcription factor that regulates the production of scopoletin. We found that
168 plants inoculated with ‘Mutualist 1’ and ‘Mutualist 2’ phenotypes retained high GUS activity,
169 which was comparable to the ancestor ($F_{5,24} = 5.6$, $P < 0.01$, Fig. 3B, Fig. S6). However, the other
170 evolved phenotypes induced a reduced GUS activity in plant relative to the mutualists (Fig. 3B,
171 Fig. S6). While the ‘Mutualist 1’ and ‘Mutualist 2’ phenotype groups included strains that showed
172 very high tolerance to scopoletin, their mean tolerance did not significantly differ from other
173 phenotype groups ($F_{5,24} = 1.76$, $P = 0.16$; Fig. 3C). However, a significant positive correlation was
174 observed between the induction of *MYB72* in *A. thaliana* roots and phenotypes’ tolerance to
175 scopoletin ($F_{1,28} = 8.29$, $P < 0.01$, Fig. 3D). This suggest that both the activation of scopoletin
176 production, and the scopoletin tolerance, were potentially under co-selection as mutualistic
177 phenotypes showed high scopoletin tolerance only when they were able to trigger increased
178 scopoletin production by the plant (upregulation of *MYB72*). Such mechanisms would have ensured
179 positive selection for mutualists relative to other evolved phenotypes.

180

181 ***Mutualistic phenotypes had mutations in genes encoding the GacS/GacA two-component***
182 ***regulatory system***

183 To gain insights into the genetic mechanisms underlying the evolution of mutualism, we performed
184 whole-genome re-sequencing of a subset of evolved isolates followed by reference-based
185 identification of point mutations (SNPs) and insertions or deletions (INDELs). These analyses
186 revealed that different evolved bacterial phenotypes were associated with relatively few mutations
187 in global regulator genes (Fig. 4) underpinning their central role in bacterial adaptation^{25,26}. While
188 only few non-parallel mutations were observed in case of ‘Ancestral-like’ and ‘Transient’
189 phenotypes (Table S2), all but two mutualistic isolates (8/10) harboured mutations in genes
190 encoding the GacS/GacA two-component system, which regulates secondary metabolism
191 alongside many other aspects of bacterial physiology²⁷. Despite high level of parallelism, a variety
192 of different mutations was observed in this locus. Three *gacS/gacA* mutations were unique to
193 ‘Mutualist 1’ isolates, and specifically associated with an uncharacterized N-terminal histidine
194 kinase domain in GacS (G27D) and the response regulatory domain of GacA (G97S; D49Y, Fig.
195 4). Four unique ‘Mutualist 2’ mutations were found upstream (at -40 of the transcription start site)
196 or inside the *gacA* coding region (E38*, D54Y and Y183S, Fig. 4). The conserved phosphate-
197 accepting aspartate 54 (D54) residue is important for phospho-relay initiated by the sensor kinase
198 GacS, and mutations of this residue are associated with complete loss-of-function²⁸⁻³⁰. Aspartate
199 49 (D49) is another conserved residue in the vicinity of D54, and the *gacA* (49Y) allele has
200 previously been reported to be associated with a partial reduction in GacA activity³⁰. The other
201 mutations in *gacA* are novel and conceivably have a significant impact on GacA activity as they
202 result in a severely truncated protein (E38*) or are located within the third recognition helix of the
203 LuxR-like tetra-helical helix-turn-helix (HTH) domain, which is known to make most of the DNA
204 contacts (Y183S)³¹. In line with the predicted effects of the mutations, ‘Mutualist 1’ isolates

205 retained part of the GacS/GacA – mediated traits, while ‘Mutualist 2’ isolates showed a severe to
206 complete disruption of secondary metabolite production (Fig. S3). These differences between
207 individual mutations are thus likely to explain the variation in life-history traits within and between
208 the ‘Mutualist 1’ and ‘Mutualist 2’ phenotype groups.

209 Several other genes were also mutated in the mutualistic isolates, including *accC* (E413K)
210 that encodes the biotin decarboxylase subunit of the acetyl coenzyme A carboxylase complex
211 involved in fatty acid biosynthesis in bacteria, and *fleQ* (R320Q) which is linked with motility and
212 biofilm formation (Fig. 4). These mutations were plant replicate line-specific, and their effect on
213 bacterial physiology or bacteria-plant interactions are unknown. Interestingly, mutualists evolved
214 in all except one selection line, which became dominated by ‘Stress-sensitive’ bacteria (Fig. 1, Fig.
215 4), that also transiently appeared in two other plant selection lines. Genetically, this phenotype was
216 mainly associated with mutations in the *rpoS* coding region and its promoter (Q65*, 3/5 of selection
217 lines). The *rpoS* gene encodes sigma factor *sigma-38*, which mediates general stress resistance^{32,33},
218 downregulates the biosynthesis of antagonistic secondary metabolites³⁴ and is involved in biofilm
219 formation³⁵ with several bacteria. In line with this, we found that ‘Stress-sensitive’ phenotypes
220 were able to form high amounts of biofilm *in vitro* (Fig. S4), which may have supported more
221 efficient root colonization³⁶ and explain their dominance in one of the plant selection lines.
222 Moreover, efficient root colonisation could have initiated a strong priority effect^{37,38}, potentially
223 constraining the subsequent emergence of mutualistic bacterial phenotypes. One of the sequenced
224 ‘Stress-sensitive’ clones had also a mutation in a TetR-family transcriptional regulator (*tetR*),
225 indicative of generalised stress tolerance evolution. Together, these results show that plant selection
226 can lead to high level of parallel evolution both at the phenotypic and molecular level.

227

228 ***The fitness benefits of GacS/GacA mutations are specific to the rhizosphere environment***

229 In order to assess whether the observed mutations specifically conferred an advantage in the
230 rhizosphere environment, we compared the fitness of evolved mutualists on plant roots and on
231 liquid growth culture media. To this end, the fitness of two evolved *gacA* (Mutualists 1 and 2; ID
232 242 and ID 220, respectively, Table S2), and one *gacS* genotype (Mutualist 1, ID 222, Table S2)
233 was compared relative to their direct ancestral genotypes without *gac* mutations (ID 133, ID 28
234 and ID 66, respectively, Table S2) within the same plant selection lines. Fitness was determined as
235 the relative competitive fitness in direct pairwise competitions as a deviation from the initial 1:1
236 ancestor-to-successor ratio *in vivo* on *A. thaliana* roots and *in vitro* in Kings' B (KB), lysogeny
237 broth (LB), and tryptic soy broth (TSB) growth media. Post-competitive genotype ratios were
238 determined using PCR-based high-resolution melting profile (RQ-HRM) analysis (see Methods
239 and Materials and Supplementary figure 7). It was found that all three *gacS/gacA* mutants had a
240 higher fitness in the rhizosphere relative to their direct ancestral genotypes without *gac* mutations
241 ($F_{3, 32} = 10.03$, $P < 0.001$, Fig. 5). Interestingly, this advantage was smaller for one of the *gacA*
242 mutants (ID 220, $F_{2, 6} = 15.35$, $P = 0.004$, Fig. 5) likely because its direct ancestor already showed
243 mutualistic behaviour due to a mutation in the *accC* gene, which likely reduced the relative benefit
244 of the *gacA* mutation within this lineage (Table S2). While the fitness benefits of *gac* mutations
245 were mainly observed in the rhizosphere, two *gac* mutants showed improved competitive fitness
246 in KB media indicative of general metabolic adaptations (genotype \times measurement environment:
247 $F_{6, 24} = 13.02$, $P < 0.001$; genotype comparisons in KB media: $F_{2, 6} = 162.6$, $P < 0.001$). Together,
248 these results confirm that the genetic changes underlying the evolution of bacterial mutualism were
249 primarily driven by plant selection.

250

251 **Discussion**

252 Even though beneficial plant-microbe interactions are widely documented, their evolutionary
253 origin is less well understood. Here we studied how an initially antagonistic relationship between
254 *P. protegens* CHA0 bacterium and its host plant, *Arabidopsis thaliana*, changed during prolonged
255 selection over six plant growth cycles (6 months). While several studies have previously reported
256 beneficial effects of CHA0 strain on plant growth in natural soils, it initially showed antagonism
257 towards the plant in our experimental conditions potentially due to production of phytotoxic
258 compounds. Crucially, this interaction rapidly evolved during the experiment leading to clear
259 phenotypic and genetic bacterial diversification and evolution of bacterial mutualists that had
260 relatively higher competitive advantage in the rhizosphere, and positive effect on the plant growth
261 compared to ancestral and other evolved bacterial phenotypes.

262 Based on our results, we suggest the following conceptual model for the evolution of
263 mutualism. As bacterial growth in this system was dependent on plant root exudates, it is likely
264 that reduction in the production of exoproducts, including lytic enzymes and antimicrobial
265 secondary metabolites (Fig. S3), by mutualists had a positive effect on plant growth and the
266 availability of plant-derived nutrients. As many metabolites produced by *Pseudomonas spp.* are
267 potentially phytotoxic²⁰, the observed shift from antagonism to mutualism could therefore be
268 explained by reduced toxicity to the plant. In turn, improved plant growth likely triggered selection
269 for mutualists that were better at competing for root exudates relative to other phenotypes, or by
270 selectively constraining the growth of non-mutualist phenotypes via certain sanctioning
271 mechanisms. As a support for this, ‘Mutualist 1’ phenotypes evolved better at growing on plant-
272 derived nutrients, while ‘Mutualist 2’ phenotypes evolved to activate plant-derived scopoletin
273 production, a compound that was relatively more harmful to non-mutualistic phenotypes. Such
274 differences between two mutualist phenotypes were also linked with subtle differences in the
275 predicted functional effects of observed *gacS/gacA* mutations. Together, these adaptations could

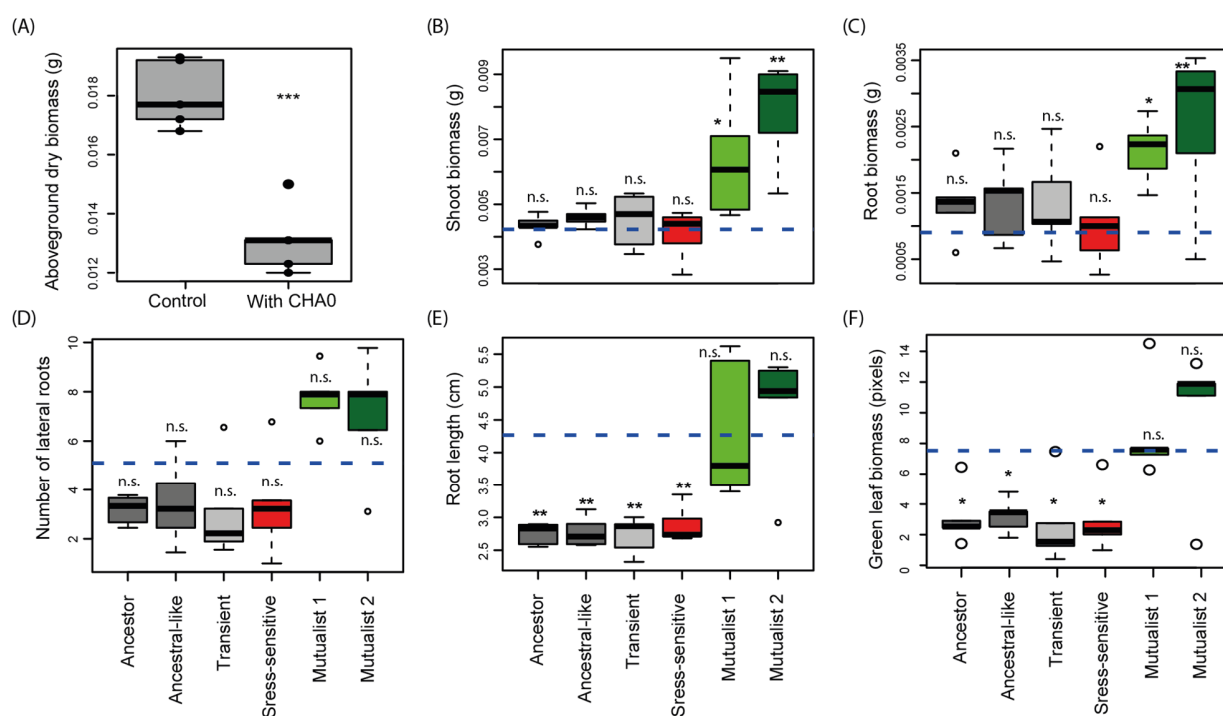
276 have created a strong selective advantage for mutualistic phenotypes as evidenced by their
277 relatively higher abundance in the rhizosphere at the end of the selection experiment.

278 At a genetic level, the evolution of mutualism could be achieved with only a few successive
279 mutations involving mainly global regulators ²⁹. This result shows an interesting parallel with
280 recent work demonstrating that the loss of a few virulence traits can turn a pathogen into a
281 beneficial symbiont ⁷. Evolution of mutualism was also linked with a clear phenotypic and
282 genotypic bacterial diversification, which has previously been observed in aquatic ³⁹ and soil ⁴⁰
283 microcosms in response to spatial heterogeneity. Here we show that such bacterial diversification
284 can also be driven by plant selection as evidenced by direct competition assays where competitive
285 benefit observed in the rhizosphere was reduced or completely absent in lab media *in vitro*.
286 Interestingly, we observed a contrasting evolutionary outcome in one of the five selection lines
287 where ‘Stress-sensitive’ genotypes were able to become dominant alongside with ‘Ancestral-like’
288 genotypes potentially due to their enhanced ability to form biofilm and colonise plant roots.
289 Interestingly, none of the phenotypes was able to reach fixation in the rhizosphere. One possibility
290 for this is that the experiment was not long enough for the selective sweeps to drive beneficial
291 mutations into fixation. Alternatively, it is possible that multiple phenotypes were able to coexist
292 due to negative frequency dependent selection or because they occupied different spatial niches as
293 seen in heterogenous soil environments ^{40,41}. These hypotheses could be studied directly in the
294 future using fluorescent microscopy and tagged strains to observe diversification and genotype
295 fluctuations in the rhizosphere both in space and time.

296 In summary, our results show that in addition to recruiting beneficial bacteria from multi-
297 species microbial communities ⁸⁻¹⁰, plants could also change the functioning of its associated
298 microbiota by creating strong selection for *de novo* evolution of mutualistic bacterial genotypes.
299 Steering bacterial evolution in the rhizosphere could thus offer plants a shortcut to improve their

300 fitness without evolving themselves⁴²⁻⁴⁴. Future work should focus on validating our findings in
301 more complex microbial communities where bacterial diversification could be also affected by
302 interactions with other microbes. In conclusion, our results call for eco-evolutionary management
303 of plant-microbe interactions in agriculture by demonstrating that plant-associated bacteria can
304 rapidly evolve along the parasitism-mutualism continuum within a few plant growing seasons.

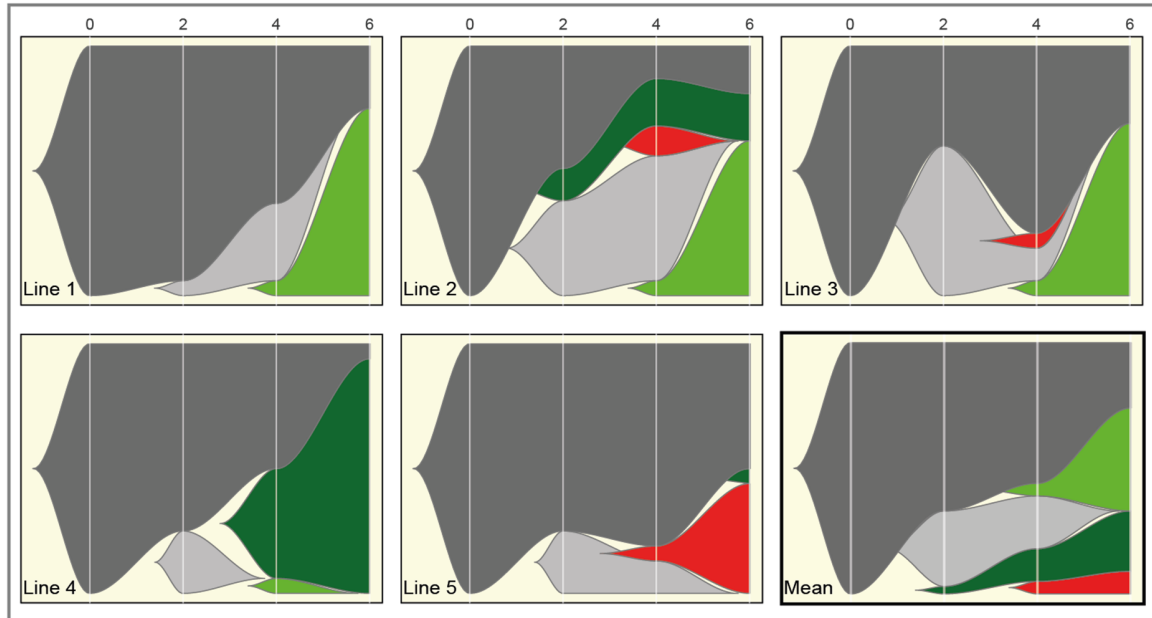
305 **Figures**
306



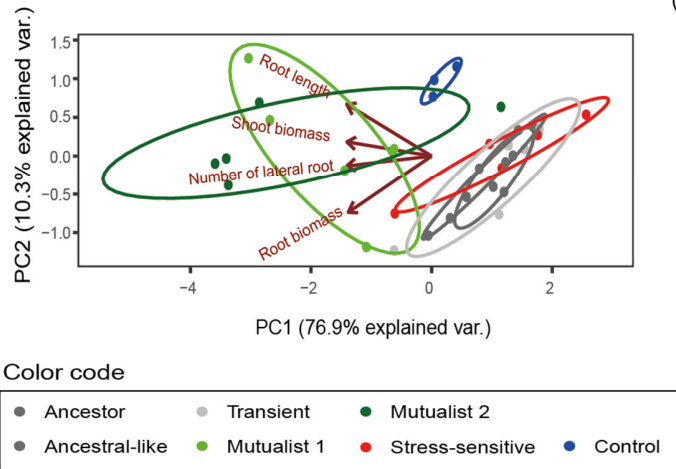
307
308 **Figure 1. Evolution of bacterial mutualism in the rhizosphere of *Arabidopsis thaliana*.** Panel
309 (A) shows the initially antagonistic effect of *Pseudomonas protegens* CHA0 on *A. thaliana* after
310 one plant growth cycle in the sterile sand study system. Panels (B-F) compare the effects of
311 ancestral and evolved *Pseudomonas protegens* CHA0 phenotypes on plant performance-related
312 traits in a separate plant growth assays performed on agar plates at the end of the selection
313 experiment. Different panels show the shoot biomass in grams (B), root biomass in grams (C),
314 number of lateral roots (D), root length in cm (E) and the amount of plant ‘greenness’ in terms of
315 green-to-white pixel ratio (F) 14 days after bacterial inoculation (Supplementary dataset 2; blue
316 dashed horizontal lines show the non-inoculated control plants). Bacterial phenotype groups are
317 displayed as different colours and were classified and named based on K-means clustering (Figure
318 S1) using 14 phenotypic traits linked to growth, stress tolerance, production of bioactive
319 compounds, and antimicrobial activity (Table S1). Boxplots show the mean effect of five
320 representative bacterial isolates from each evolved phenotype in addition to ancestor isolates (See
321 Table S2). Statistical testing in all panels was carried out using ANOVA, and asterisks above plots
322 indicate significant differences between control plants and bacteria-treated plants (* $\alpha=0.05$,
323 ** $\alpha=0.01$, *** $\alpha=0.001$; n.s. = non-significant).

324

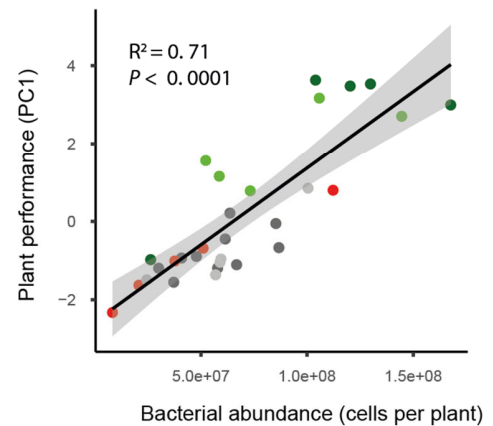
(A)



(B)



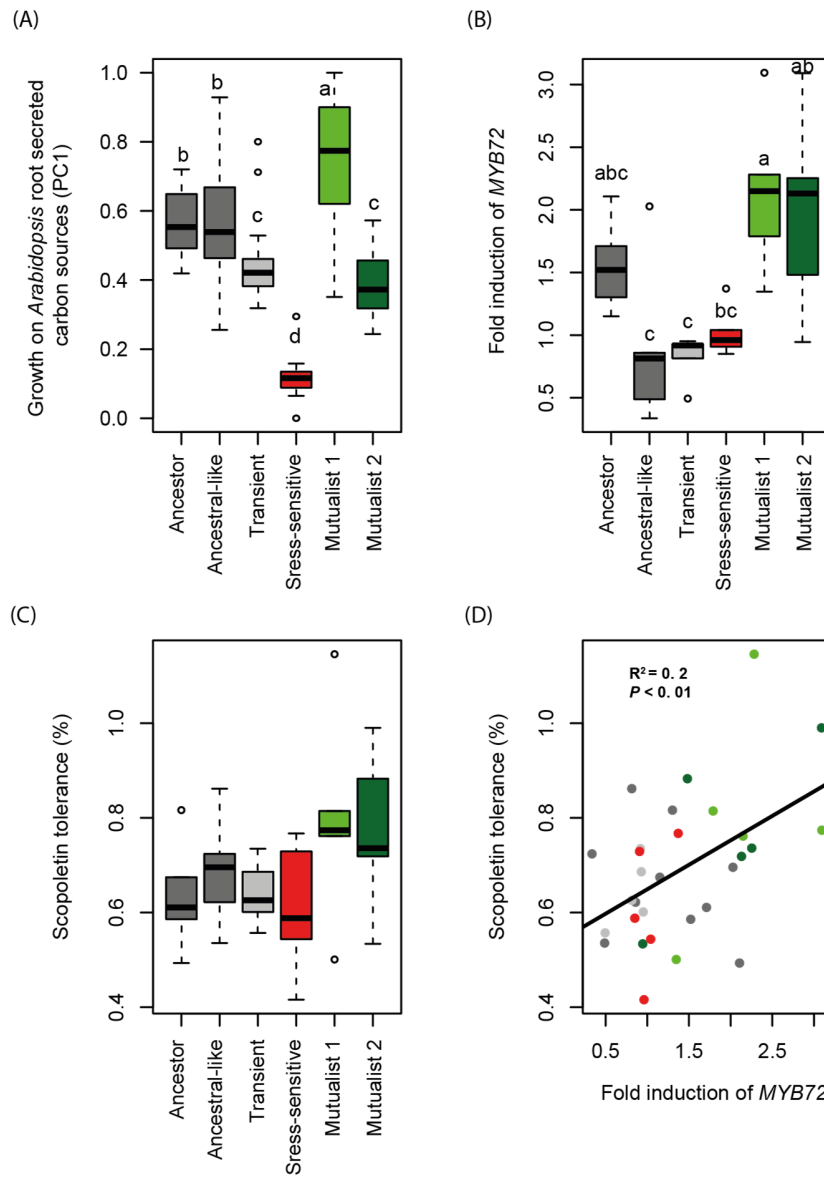
(C)



325
326 **Figure 2. Temporal changes in bacterial phenotypes during the selection experiment and**
327 **positive correlation between evolved bacteria and plant growth.** Panels in A show the dynamics
328 of five bacterial phenotype groups across five plant replicate lines and the overall mean pattern
329 during six growth cycles (6 months). The x-axis shows the plant growth cycle (0: ancestral
330 bacterium), and the y-axis shows the relative abundance of each bacterial phenotype. Panel (B)
331 shows a principal component analysis (PCA) for five representative bacterial isolates from each

332 evolved phenotype group in addition to ancestor isolates (See Table S2) based on their plant
333 growth-related traits. The negative PC1 values of each isolate were extracted and combined to a
334 ‘Plant performance’ index, which included bacterial effects on shoot biomass, root biomass and
335 root architecture explaining 76.9% of the total variation in plant growth. Panel (C) shows a positive
336 correlation between ‘Plant performance’ and bacterial abundance in the plant roots at the end of
337 the fitness assays.

338
339



340

341 **Figure 3. Selection mechanisms favouring the increase in the relative abundance of**

342 **mutualists in the rhizosphere of *Arabidopsis thaliana*.** Panel (A) shows the growth of ancestor

343 and evolved *Pseudomonas protegens* CHA0 phenotypes on carbons typically secreted by *A.*

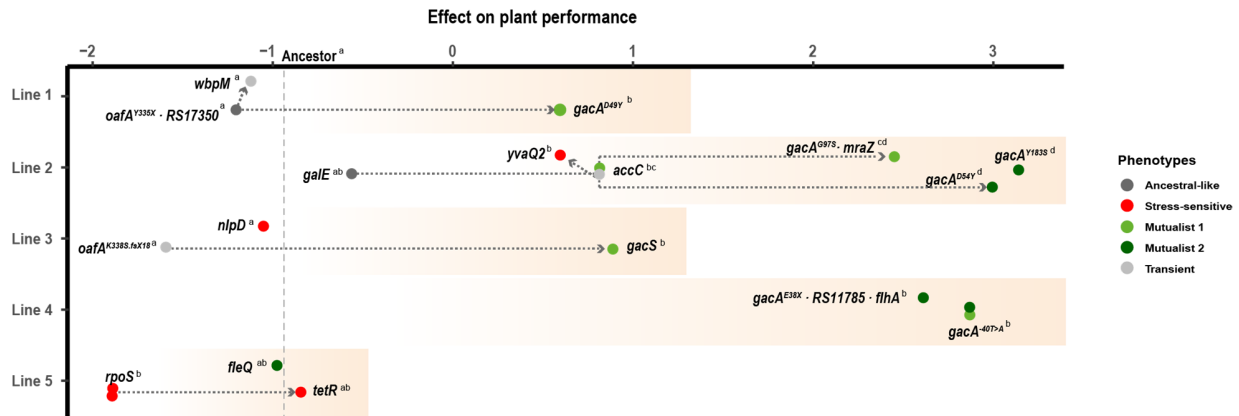
344 *thaliana* (14 most dominant carbons analysed as a combined index based on normalised first

345 principal component (PC1, which explained 83.9 % of total variation); in total, 16 ancestral, 119

346 ‘Ancestral-like’, 11 ‘Stress-sensitive’, 37 ‘Mutualist 1’, 31 ‘Mutualist 2’ and 41 ‘Transient’ isolates

347 were characterized, Supplementary dataset 1). Panel (B) shows the effect of ancestor and evolved
348 *P. protegens* CHA0 phenotypes on the expression of *MYB72* (transcription factor responsible for
349 scopoletin production) in the roots of a GUS *A. thaliana* reporter line (based on the quantification
350 of GUS staining of the roots, Fig. S6). Panel (C) shows the relative growth of ancestor and evolved
351 *P. protegens* CHA0 phenotypes in the presence of the plant-secreted scopoletin antimicrobial at 2
352 mM concentration after 96 hrs of incubation relative to no-scopoletin control. Panel (D) shows a
353 positive relationship between *MYB72* expression (fold induction; x-axis) and scopoletin tolerance
354 (y-axis) for all tested isolates. Panels (B-D) include five representative bacterial isolates from each
355 phenotype in addition to the ancestor (each replicate line represented; See Table S2). In all panels,
356 colours represent different phenotype groups and statistical testing in panels (A-C) was carried out
357 using ANOVA (different letters indicate significant differences based on a Tukey HSD test
358 ($\alpha=0.05$)).

359

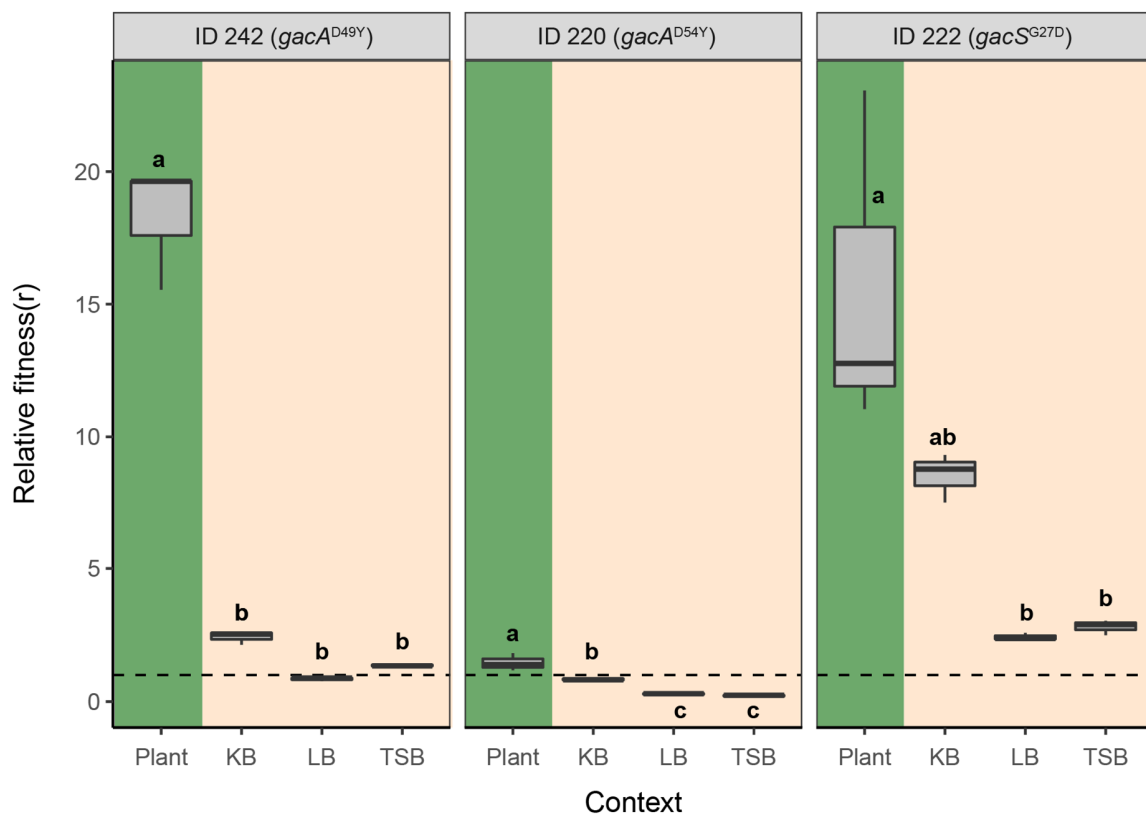


Bacterial phenotype	Plant replicate line	Mutation	Protein function	
Mutualist 1	Line 1	<i>gacA</i> (D49Y)	Two-component regulator	360
	Line 2	<i>gacA</i> (Y97S)	Two-component regulator	361
		<i>mraZ</i> (upstream(221bp))	Transcriptional regulator MraZ	
		<i>accC</i> (E413K)	Biotin carboxylase	
Line 3	<i>gacS</i> (G27D)	Two-component regulator		
Mutualist 2	Line 2	<i>gacA</i> (Y183S)	Two-component regulator	362
		<i>gacA</i> (D54Y)	Two-component regulator	
	Line 4	<i>gacA</i> (upstream (40 bp))	Two-component regulator	363
		<i>gacA</i> (E38X)	Two-component regulator	
		<i>RS11785</i> (S256C)	LysR family transcriptional regulator	
Line 5	<i>flhA</i> (H393Q.fsX15)	Flagellar biosynthesis protein FlhA		
	<i>fleQ</i> (R320Q)	Sigma-54-dependent Fis family transcriptional regulator		
Stress-sensitive	Line 2	<i>yvaQ2</i> (upstream (9 bp))	Methyl-accepting chemotaxis protein	364
	Line 3	<i>nlpD</i> (Q197P)	LysM, promotor for <i>rpoS</i>	
	Line 5	<i>rpoS</i> (Q65X)	Sigma-38, stress regulon	365
<i>tetR</i> (Y127X)		TetR family transcriptional regulator		

366

367 **Figure 4. Genetic basis of bacterial evolution in the rhizosphere of *Arabidopsis thaliana*.** Clear
 368 parallel evolution was observed between four out five plant replicate selection lines based on re-
 369 sequencing of 25 evolved and five ancestor isolates used in the phenotypic assays. Filled dots
 370 represent isolates with non-synonymous mutations (present in 18/25 evolved isolates), and the x-
 371 axis shows a combined index of ‘Plant performance’ relative to non-inoculated control plants
 372 (values on the x-axis indicate positive and negative effects on the plant and the y-axis shows the
 373 five independent plant replicate selection lines). The effect of the ancestral bacterial genotype on
 374 plant performance is shown as a vertical dashed line. The different letters on the top right of each

375 genotype indicate significant differences based on a Tukey HSD test ($\alpha=0.05$; each line analysed
376 separately). The accumulation of mutations within replicate lines are shown with connected dashed
377 arrows. The table lists unique mutations (and the strains' ID number) linked with evolved bacterial
378 phenotypes, and additional mutations that appeared later during the experiment within the same
379 genetic background are shown after the indent; notably, these additional mutations did not affect
380 the bacterial phenotypes (See Table S3 for a more detailed description of the mutations).



381
382 **Figure 5. Competitive fitness of *gac* mutants relative to their direct ancestors in the**
383 **rhizosphere and in *in vitro* culture media.** The *gac* mutants' relative fitness (*r*) was calculated
384 based on the deviation from the initial 1:1 genotype ratio (dashed line) after direct competition in
385 different environments. Fitness values above the dashed line indicate a relatively higher
386 competitive advantage of *gac* mutants relative to their ancestral genotypes without *gac* mutations

387 (Table S2), whereas values below the dashed line denote for decreased competitive ability of
388 evolved *gac* mutants. In all panels, green and beige backgrounds denote competition assays
389 conducted in the rhizosphere and in standard culture media, respectively. Different small letters
390 above the boxplots represent significant differences in *r* between growth conditions for each mutant
391 based on three biological replicates (one-way ANOVA, Tukey's HSD test, $\alpha=0.05$).
392

393 **Materials and Methods**

394 **Bacterial strain and growth conditions**

395 We used *Pseudomonas protegens* (formerly *Pseudomonas fluorescens*)⁴⁵ CHA0 as a model strain,
396 which was initially isolated from tobacco roots⁴⁶. The strain was chromosomally tagged with GFP
397 and a kanamycin resistance cassette to enable specific tracking of the strain and detection of
398 contaminations¹⁹. This bacterium has the genetic potential to produce various bioactive
399 metabolites, including the plant hormone indole-3-acetic acid (IAA), antimicrobial compounds and
400 lytic enzymes⁴⁷. Prior to the experiment, bacteria were grown for 48 h on a King's medium B⁴⁸
401 (KB) agar plate supplemented with 50 $\mu\text{g ml}^{-1}$ kanamycin, a single colony was randomly picked
402 and grown for 12 h in KB at 28 °C with agitation. The cell culture was then washed for three times
403 in 10 mM MgSO_4 and adjusted to 10^7 cells ml^{-1} and used as inoculant for all plants. This inoculant
404 was also stored at -80 °C as frozen ancestral stock, from which 'Ancestor' isolates were picked in
405 later experiments.

406

407 **Host plant and growth conditions**

408 We used *Arabidopsis thaliana* ecotype Col-0 as a model host plant. Surface-sterilized seeds were
409 first sown in Petri dishes with agar-solidified (1.5% agar (w/v)) modified Hoagland's medium:
410 (KNO_3 (3 mM), MgSO_4 (0.5 mM), CaCl_2 (1.5 mM), K_2SO_4 (1.5 mM), NaH_2PO_4 (1.5 mM), H_3BO_3
411 (25 μM), MnSO_4 (1 μM), ZnSO_4 (0.5 μM), $(\text{NH}_4)_6\text{Mo}_7\text{O}_{24}$ (0.05 μM), CuSO_4 (0.3 μM), MES (2.5
412 mM) and 50 μM Fe(III)EDTA, pH = 5.8) and stratified for 2 days at 4 °C after Petri dishes were
413 positioned vertically and transferred to a growth chamber (20 °C, 10 h light/14 h dark, light
414 intensity 100 $\mu\text{mol m}^{-2} \text{sec}^{-1}$). After two weeks of incubation, two seedlings were transferred to

415 closed and sterile ECO2 boxes (http://www.eco2box.com/ov80xxl_nl.htm) for selection
416 experiment. The ECO2 boxes were filled with 260 g of dry, carbon-free silver sand that was
417 previously washed with MilliQ water to remove dissolvable chemical elements and heated to 550
418 °C for 24 h to remove remaining organic material. Prior to transplantation the sand was amended
419 with 13 ml of modified Hoagland medium.

420

421 **Design of the selection experiment**

422 The selection experiment was conducted in a gnotobiotic system to remove confounding effects
423 that may emerge as a result of competitive interactions with other micro-organisms, and to place
424 the focus on plant-mediated selective pressures. Moreover, we allowed only the bacteria to evolve
425 during the experiment and used new clonal plants at every bacterial transfer. We set up five
426 independent plant-bacterium replicate lines, which were grown for six independent plant growth
427 cycles (see Figure S1 for an overview of the experimental design). The experiment was started by
428 inoculating 10^6 cells of the stock *P. protegens* CHA0 culture (From here on abbreviated as
429 “ancestor”) into the rhizosphere of two-week-old *A. thaliana* seedlings growing in sterile silver
430 sand within ECO2 boxes (two plants per replicate selection line). Inoculated plants were then
431 grown for four weeks (20 °C, 10 h light/14 h dark, light intensity $100 \mu\text{mol m}^{-2} \text{sec}^{-1}$) after which
432 the plant growth cycle was terminated and root-associated bacteria were harvested by placing the
433 roots of both plants into a 1.5 ml Eppendorf tubes filled with 1 ml 10 mM MgSO_4 and two glass
434 beads. Rhizosphere bacteria were suspended into the liquid using TissueLyser II at a frequency of
435 20 s^{-1} for 1 min after which bacterial cell densities were determined using flow cytometry (BD
436 Accuri™ C6 Plus, thresholds for FSC: 2000, SSC: 8000). After this, 10^6 cells were inoculated to
437 the rhizosphere of new *A. thaliana* plants to initiate the next plant growth cycle. Possible

438 contaminations were checked by plating the suspension on 3 g l⁻¹ tryptic soy agar (TSA) plates and
439 it was verified that all colonies carried the *GFP* marker gene, as observed under UV light.

440
441 **Bacterial life-history traits measurements**
442 Individual bacterial colonies were isolated from all replicate plant selection lines for life-history
443 measurements at the end of the second, fourth and sixth plant growth cycle by dilution plating the
444 rhizosphere suspension on 3 g l⁻¹ TSA plates. After incubation at 28 °C for 24 h, 16 colonies were
445 randomly picked from each replicate selection lines resulting in a total of 240 evolved and 16
446 ancestral colonies. All these colonies were characterized for a set of key bacterial life-history traits
447 representative of growth, stress resistance and traits linked with plant-microbe interactions.

448 ***a. Bacterial growth yield in KB medium***

449 All the bacterial isolates were grown in 96-well plates with 160 µl 1/3 strength liquid KB, at 20 °C
450 without shaking. Bacterial yield was determined as the maximum optical density at 600 nm after
451 three days of growth using a spectrophotometer (SPECTROstar Nano).

452 ***b. Bacterial stress resistance***

453 We measured bacterial resistance to a range of different stresses using various 96-well microplate
454 assays. Abiotic stress resistance was determined by growing bacteria in 160 µl of 1 g l⁻¹ tryptic soy
455 broth (TSB) containing 0.0025% H₂O₂ (oxidative stress), 15% polyethylene glycol (PEG)-6000
456 (water potential stress) or 2% NaCl (salt stress). We used resistance to antibiotics commonly
457 produced by rhizosphere microorganisms as indicator of biotic stress resistance. Antibiotic
458 resistance was tested in 160 µl of 1 g l⁻¹ TSB supplemented with 1 µg ml⁻¹ streptomycin, 1 µg ml⁻¹
459 tetracycline, or 5 µg ml⁻¹ penicillin, respectively. Bacterial growth with and without stresses were
460 determined after three days of growth at 20 °C without shaking as optical density at 600 nm and

461 stress resistance defined as the ratio of bacterial growth in the stressed relative to the non-stressed
462 control treatment.

463 ***c. Traits linked with plant-microbe interactions***

464 *P. protegens* CHA0 harbours several traits that are linked to plant growth including production of
465 antibiotics and plant hormones. To assess these traits, we grew each bacterial colony in 96-well
466 plates containing 160 μ l of 1/3 strength liquid KB per well at 20 °C with agitation for 72 h. Cell-
467 free supernatants were obtained by filter sterilization (0.22 μ m) using Multiscreen HTS 96-well
468 filtration plates (1000 \times g, 30 min), which were used to measure the production of the plant
469 hormone auxin (Indole-3-acetic acid (IAA)), iron-chelating siderophores and proteolytic activity.
470 Furthermore, we also measured antifungal and antibacterial activity of all colonies.

471 **IAA detection:** The production of the plant hormone auxin was determined with a colorimetric
472 test ⁴⁹. Briefly, 30 μ l *P. protegens* CHA0 cell-free filtrate was incubated with 30 μ l R1 reagent (12
473 g l⁻¹ FeCl₃, 7.9 M H₂SO₄) for 12 h in the dark and optical density read at 530 nm of the colorimetric
474 complex was used as a measurement of IAA concentration.

475 **Siderophore activity:** Iron chelating ability was measured as a proxy for siderophore production
476 ⁵⁰. To this end, 100 μ l of *P. protegens* CHA0 cell-free filtrate was mixed with 100 μ l of modified
477 CAS solution (with 0.15 mM FeCl₃) and optical density read at 630 nm after 3 hours of incubation
478 was used as a proxy of siderophore production. The iron chelating ability was calculated based on
479 the standard curve based on modified CAS assay solution with a range of iron concentration (0,
480 0.0015, 0.003, 0.006, 0.009, 0.012, 0.015 mM FeCl₃).

481 **Proteolytic activity:** The proteolytic activity assay we used was adapted from Smeltzer et al.
482 (1993) ⁵¹. Briefly, 15 μ l of *P. protegens* CHA0 cell-free filtrate was incubated with 25 μ l of

483 azocasein (2% w/v in 50 mM Tris-HCl pH 8.0) at 40 °C for 24 hours. 125 µl of 10% w/v cold
484 trichloroacetic acid (TCA) was added to precipitate superfluous azocasein, and then 100 µl
485 supernatant was neutralized with 100 µl of 1M NaOH after centrifugation at 5000 rpm for 30
486 minutes. Optical density read at 440 nm was used as a proxy of exoprotease activity.

487 **Tryptophan side chain oxidase (TSO) activity:** TSO activity, an indicator of quorum sensing
488 activity in *P. protegens* CHA0, was measured based on an modified established colorimetric assay
489 ⁵²: Three-day-old bacterial cultures grown in 1/3 strength liquid KB were mixed at a 1:1 ratio with
490 a reagent solution (5 g l⁻¹ SDS, 37.6 g l⁻¹ glycine 2.04 l⁻¹ g tryptophan, pH 3.0) and TSO activity
491 was measured as optical density at 600 nm after overnight incubation.

492 **Biofilm formation:** We quantified bacterial biofilm formation using a standard protocol ⁵³. Briefly,
493 bacteria were grown at 20 °C for 72h in 160 µl 1 g l⁻¹ TSB in 96-well microtiter plate with TSP lid
494 (TSP, NUNC, Roskilde, Denmark). Planktonic cells were removed by immersing the lid with pegs
495 three times in phosphate-buffered saline solution (PBS). Subsequently, the biofilm on the pegs was
496 stained for 20 minutes in 160 µl 1% Crystal Violet solution. Pegs were washed five times in PBS
497 after which the Crystal Violet was extracted for 20 minutes from the biofilm in a new 96-well
498 microtiter plate containing 200 µl 96% ethanol per well. Biofilm formation was defined as the
499 optical density at 590 nm of the ethanol extracted Chrystal Violet ⁵⁴.

500 **Inhibition of other microorganisms:** Antimicrobial activity was defined as the relative growth of
501 the target organism in *P. protegens* supernatant compared to the control treatment. Antifungal
502 activity of the cell-free supernatant was assessed against the ascomycete *Verticillium dahlia*. The
503 fungus was grown on potato dextrose agar (PDA) at 28 °C for 4 days, after which plugs of fungal
504 mycelium were incubated in potato dextrose broth (PDB) medium at 28 °C and gentle shaking for
505 5 days. Fungal spores were collected by filtering out the mycelium from this culture over glass

506 wool. Subsequently, spores were washed and resuspended in water and the OD₅₉₅ of the suspension
507 was adjusted to 1. Five μ l of this spore suspension was then inoculated with 15 μ l *P. protegens*
508 CHA0 cell-free filtrate and incubated in 160 μ l of 1 g l⁻¹ PDB medium for 2 days at 20 °C in 96
509 well plates. Fungal growth was measured as optical density at 595 nm after 2 days of growth and
510 contrasted with the growth in the control treatment (PDB medium without *P. protegens*
511 supernatant). Antibacterial activity was determined using the plant pathogen *Ralstonia*
512 *solanacearum* as a target organism. *R. solanacearum* was grown in 160 μ l of 1 g l⁻¹ TSB medium
513 supplemented with 15 μ l of *P. protegens* CHA0 cell-free filtrate or 15 μ l of 1/3 strength liquid KB
514 as a control for 2 days at 20 °C. *R. solanacearum* growth was measured as optical density at 600
515 nm.

516

517 **Determining changes in *P. protegens* CHA0 interactions with *A. thaliana* after** 518 **the selection experiment**

519 Based on the life-history trait measurements, five distinct bacterial phenotypes were identified
520 using K-means clustering analysis (Fig S2). In order to assess whether phenotypic changes
521 reflected shifts in the strength and type of plant-bacterium interaction, we chose five isolates from
522 each bacterial phenotype group representing each replicate selection line and five ancestral isolates
523 for further measurements (a total of 30 isolates, Table S2).

524

525 **a. Effects of ancestor and evolved bacteria on plant performance**

526 For each isolate we measured root colonizing ability and impact on plant performance. All 30
527 bacterial isolates were incubated overnight in 1/3 KB strength liquid at 20 °C. The culture was
528 centrifuged twice for five minutes at 5000 x g and the pellet was washed and finally resuspended

529 in 10 mM MgSO₄. The resulting suspension was adjusted to an OD₆₀₀ of 0.01 for each strain as
530 described previously⁵⁵. Ten µl of the bacterial suspension (or 10 mM MgSO₄ as a control) was
531 applied to the roots of three 10-day old sterile *Arabidopsis thaliana* Col-0 seedlings (excluding 2-
532 days of stratification at 4 °C) grown on vertically positioned Petri dishes with agar-solidified (1.5%
533 agar (w/v)) modified Hoagland's medium (n = 3 biological plant replicates, each containing 3
534 seedlings). Plants were grown for 14 days before harvesting. Plants were photographed before and
535 14 days after bacterial inoculation.

536 Bacterial effects on plant health were quantified as leaf 'greenness' as the presence of
537 ancestral strain was observed to lead to bleaching and loss of chlorophyll in *A. thaliana* leaves. The
538 'greenness' was quantified from photographs by measuring the number of green pixels. To this
539 end, photographs were first transformed in batch using Adobe Photoshop 2021 by sequentially
540 selecting only green areas followed by thresholding balancing green tissue over background noise
541 (Level 80). This resulted in black-and-white images for further analysis, and the mean number of
542 white pixels per fixed-sized region-of-interest of the aboveground tissue was subsequently
543 determined as 'greenness' using ImageJ. The numbers of lateral roots and the primary root length
544 were also measured using ImageJ (version 1.50i). The root morphology data measured at the end
545 of the experiment was normalized with the data collected at the time of inoculation for each
546 individual seedling.

547 To determine shoot biomass, the rosette of each plant was separated from the root system
548 with a razor blade and weighted. The roots were placed into a pre-weighted 1.5 ml Eppendorf tubes
549 to quantify the root biomass. Then these tubes were filled with 1 ml 10 mM MgSO₄ buffer solution
550 and two glass beads. The rhizosphere bacteria were suspended into buffer solution using
551 TissueLyser II at a frequency of 20 s⁻¹ for 1 min after which bacterial densities were determined
552 using flow cytometry as described above.

553 Shoot biomass, root biomass, root length, and number of lateral roots were used in a
554 principal component analysis (PCA) to calculate an overall impact of the bacteria on plant
555 performance (Fig 2E). The first principal component (PC1) explained 79.9% of the variation and
556 was normalized against the control treatment to be used as a proxy of ‘Plant performance’ in which
557 positive values reflect plant growth promotion and negative values plant growth inhibition.

558 ***b. Root derived carbon source utilization***

559 To measure changes in bacterial growth on potential root derived carbon sources, we measured the
560 growth of all 256 isolates using modified Ornston and Stanier (OS) minimal medium ⁵⁶
561 supplemented with single carbon sources at a final concentration of 0.5g l⁻¹ in 96-well plates
562 containing 160 µl carbon supplemented OS medium per well. The following carbon sources were
563 selected based on their relatively high abundance in *Arabidopsis* root exudates²¹: alanine,
564 arabinose, butyrolactam, fructose, galactose, glucose, glycerol, glycine, lactic acid, putrescine,
565 serine, succinic acid, threonine and valine. Bacterial growth was determined by measuring optical
566 density at 600 nm after three days incubation at 20 °C.

567 ***c. GUS histochemical staining assay and bacterial growth under scopoletin stress***

568 To investigate effects of the ancestor and evolved strains of *P. protegens* CHA0 on expression of
569 *MYB72* gene, we applied *GUS* histochemical staining assay to the 30 selected isolates (Table S2).
570 *MYB72* is a transcription factor involved in production of the coumarin scopoletin in *Arabidopsis*
571 roots and specific rhizobacteria can upregulate expression of *MYB72* in the roots. Scopoletin is an
572 iron-mobilizing phenolic compound with selective antimicrobial activity ²². Seedlings of the *A.*
573 *thaliana* *MYB72_{pro}:GFP-GUS* ²⁴ reporter line were prepared as described above. Seven day old
574 seedlings were inoculated directly below the hypocotyls with 10 µl of a bacterial suspension
575 (OD₆₆₀ = 0.1) as described previously ²⁴. At 2 days after inoculation, the roots were separated

576 from the shoots and washed in Milli-Q water (Millipore Corp., Bedford, MA) to remove all the
577 adhered bacteria. GUS staining of the roots was performed in 12-well microtiter plates where each
578 well contained roots of 5 to 6 seedlings and 1 mL of freshly prepared GUS substrate solution (50
579 mM sodium phosphate with a pH at 7, 10 mM EDTA, 0.5 mM K₄[Fe(CN)₆], 0.5 mM
580 K₃[Fe(CN)₆], 0.5 mM X-Gluc, and 0.01% Silwet L-77) as described previously⁵⁷. Plates were
581 incubated in the dark at room temperature for 16 h. The roots were fixed overnight in 1mL
582 ethanol:acetic acid (3:1 v/v) solution at 4 °C and transferred to 75% ethanol. Then the pictures of
583 each microtiter plates were taken, and GUS activity was quantified by counting the number of blue
584 pixels in each well of the microtiter plates using image analysis in ImageJ (version 1.52t). To assess
585 the effects of scopoletin on ancestral and evolved *P. protegens* CHA0 isolates, we applied a
586 sensitivity assay to the 30 selected isolates (Table S2). In brief, growth of bacterial isolates was
587 measured in 1 g l⁻¹ TSB medium (160 µl) supplemented with scopoletin at final concentrations of
588 0 µM (control), 500 µM, 1000 µM, and 2 mM using optical density at 600 nm after 96 h incubation
589 at 20 °C without shaking in 96-well microtiter plates. Maximal effect (E_{max}) of scopoletin was
590 calculated via R package ‘GRmetrics’⁵⁸ as an indication of scopoletin tolerance.

591

592 **Whole genome sequencing**

593 All 30 isolated phenotypes were whole genome sequenced to identify possible mutations and
594 affected genes. To this end, isolates were cultured overnight at 28 °C in 1/3 strength liquid KB.
595 Chromosomal DNA was isolated from each culture using the GenElute™ Bacterial Genomic DNA
596 Kit Protocol (NA2100). DNA samples were sheared on a Covaris E-220 Focused-ultrasonicator
597 and sheared DNA was then used to prepare Illumina sequencing libraries with the NEBNext®
598 Ultra™ DNA Library Prep Kit (New England Biolabs. France) and the NEBNext® Multiplex

599 Oligos for Illumina® (96 Index Primers). The final libraries were sequenced in multiplex on the
600 NextSeq 500 platform (2 x 75 bp paired-end) by the Utrecht Sequencing Facility
601 (<http://www.useq.nl>) yielding between 1.0 and 6.4 million reads per sample equivalent to ~10 – 70
602 fold coverage (based on comparison with the original 6.8 Mbp reference genome NCBI GenBank:
603 [CP003190.1](#)).

604

605 **Variant calling analysis**

606 We first constructed an updated reference genome of *P. protegens* CHA0, carrying the *GFP* marker
607 gene on its chromosome, from the ancestral strain using the A5 pipeline with default parameters
608 ⁵⁹. The input dataset for this sample consisted of 3,1 M reads and totals an approximate 34-fold
609 coverage. The size of the updated reference genome is 6.8 Mbp, with a G+C content of 63.4%, and
610 it comprises 80 scaffolds, with a N_{50} value of 343 Kbp. We subsequently used PROKKA ⁶⁰ (version
611 1.12; <https://github.com/tseemann/prokka>) for full annotation of the updated reference genome,
612 and this resulted in the identification of 6,147 genes. The updated genome is deposited in NCBI
613 GenBank with following reference: [RCSR000000000.1](#).

614 Having established the ancestral genome sequence, we subsequently used Snippy (version
615 3.2-dev; <https://github.com/tseemann/snippy>) to identify and functionally annotate single
616 nucleotide polymorphisms and small insertions and deletions (indels) for each individual strain. In
617 addition, we investigated the breadth of coverage for each gene per sample with BedTools ⁶¹ to
618 identify genes with large insertions or deletions. An overview of the polymorphisms is shown in
619 Supplementary Table S3. Raw sequencing data for this study is deposited at the NCBI database
620 under BioProject [PRJNA473919](#).

621

622 **Relative competitive fitness of *gac* mutants measured *in vivo* and *in vitro***

623 The relative competitive fitness of selected *gac* mutants was measured in direct competition with
624 their direct ancestors both *in vivo* in the rhizosphere of *A. thaliana* and *in vitro* in different standard
625 culture media. Relative fitness was measured as deviation from initial 1:1 ratio of bacterial clone
626 pairs based on PCR-based high-resolution melting profile (RQ-HRM) analysis. Three pairs of
627 isolates were selected: A) Evolved *gacA* ID 242 (genotype *oafA*^{Y335X} · *RS17350*^{A77A.fsX14} ·
628 *gacA*^{D49Y}) and its direct ancestral genotype 133 (genotype *oafA*^{Y335X} · *RS17350*^{A77A.fsX14}) from
629 evolutionary line 1; B) Evolved *gacA* ID 220 (genotype *galE*^{V32M} · *accC*^{E413K} · *gacA*^{D54Y}) and its
630 direct ancestral genotype 28 (genotype *galE*^{V32M} · *accC*^{E413K}) from line 2; C) Evolved *gacS* ID 222
631 (genotype *oafA*^{K338S.fsX18} · *gacS*^{G27D}) and its direct ancestral genotype 66 (genotype *oafA*^{K338S.fsX18})
632 from line 3. Bacterial isolates were first grown overnight in KB medium at 28 °C, centrifuged at
633 4,500 rpm for 10 min and the pellet resuspended in 10 mM MgSO₄. This washing procedure was
634 repeated twice. The resulting bacterial suspensions were diluted to OD₆₀₀ = 0.05. The initial
635 inoculum for the competition assays was then generated by mixing equal volumes of evolved and
636 ancestral competitors in a ratio of 1:1.

637

638 *Measuring competitive fitness in A. thaliana rhizosphere*

639 This assay was performed on the roots of 10-day old *A. thaliana* seedlings grown on full strength
640 Hoagland agar plates, which were prepared as described earlier. Twenty µl of the initial inoculum,
641 containing a total of 10⁶ bacterial cells, was inoculated on to the root-shoot junction of each
642 seedling. After 14 days of growth, bacterial populations were isolated from the roots as described
643 earlier and stored at -80 °C in 42.5% glycerol for relative abundance measurements.

644

645 *Measuring competitive fitness in culture media*

646 Competition assays were also performed in three commonly used nutrient-rich growth media:
647 Kings' B (KB), lysogeny broth (LB), and tryptic soy broth (TSB). KB contained 20 g proteose
648 peptone, 1.5 g MgSO₄·7H₂O, 1.2 g KH₂PO₄ and 10 g glycerol per litre and the pH was adjusted to
649 7.3 ± 0.2. TSB contained 30 g tryptic soy broth per litre and pH was adjusted to 7.3 ± 0.2. LB
650 contained 10 g peptone, 5 g yeast extract and 5 g NaCl per litre. Twenty µl inoculum of competing
651 strains, containing about 10⁶ bacterial cells, were added into wells containing 140 µl fresh medium
652 in a 96-well plate. The microplates were incubated at 28 °C without shaking for 48 after 80 µl
653 sample was harvested and stored at -80 °C in 42.5% glycerol from each well for relative abundance
654 measurements.

655

656 *RQ-HRM assay for quantifying changes in genotype frequencies after competition*

657 We used a High-Resolution Melting (HRM) curve profile assay with integrated LunaProbes to
658 quantify the ratio of mutant to wild type genotypes⁶²⁻⁶⁴. The probes and primers used in this study
659 are listed in Table S4. Primers were designed using Primer3. Probes were designed with the single
660 nucleotide polymorphism (SNP) located in the middle of the sequence, and the 3' end was blocked
661 by carbon spacer C3. The primer asymmetry was set to 2:1 (excess primer: limiting primer) in all
662 cases. Pre-PCR was performed in a 10-µl reaction system, with 0.25 µM excess primer, 0.125 µM
663 limiting primer, 0.25 µM probe, 0.5 µl bacterial sample culture (100-fold diluted saved sample,
664 OD₆₀₀ is about 0.01), 1X LightScanner Master Mix (BioFire Defense). DMSO with the final
665 concentration 5% was supplemented in all reactions to ensure the targeted melting domains are
666 within the detection limit of the LightScanner (Idaho Technology Inc.). Finally, MQ water was
667 used to supplement up to 10 µl. A 96-well black microtiter plate with white wells was used to

668 minimize background fluorescence. Before amplification, 25 μ l mineral oil was loaded in each well
669 to prevent evaporation, and the plate was covered with a foil seal to prevent the degradation of
670 fluorescent molecules. Amplification was initiated by a holding at 95 $^{\circ}$ C for 3 min, followed by 55
671 cycles of denaturation at 95 $^{\circ}$ C for 30 s, annealing at 60 $^{\circ}$ C for 30 s and extension at 72 $^{\circ}$ C for 30
672 s and then kept at 72 $^{\circ}$ C for 10 min. After amplification, samples were heated in a ThermalCycler
673 (Bio-Rad) shortly to 95 $^{\circ}$ C for 30 s to denature all double-stranded structures followed by a rapid
674 cooling to 25 $^{\circ}$ C for 30 s to facilitate successful hybridization between probes and the target strands.
675 The plate was then transferred to a LightScanner (Idaho Technology Inc.). Melting profiles of each
676 well were collected by monitoring the continuous loss of fluorescence with a steady increase of the
677 temperature from 35 $^{\circ}$ C to 97 $^{\circ}$ C with a ramp rate of 0.1 $^{\circ}$ C /s. The relative quantification was
678 based on the negative first derivative plots using software MATLAB. The areas of probe-target
679 duplexes melting peaks were auto-calculated by 'AutoFit Peaks I Residuals' function in software
680 PeakFit (SeaSolve Software Inc.). The mutant frequency X was calculated using the formula shown
681 below:

$$682 \quad X = \frac{\text{Area}_{mutant}}{\text{Area}_{mutant} + \text{Area}_{WT}}$$

683 To validate the RQ-HRM method, standard curves were generated by measuring mixed samples
684 with known proportions of mutant templates: 0%, 10%, 20%, 30%, 40%, 50%, 60%, 70%, 80%,
685 90% and 100%. Measurements for each sample were done in triplicate. Linear regression formula
686 of each mutant between actual frequencies and measured frequencies were shown in Figure S7.
687 The high R^2 values, and nearly equal to 1 slope values of these equations, confirmed that the RQ-
688 HRM method can accurately detect mutants' frequency in a mixed population.

689 The relative fitness of the evolved strains was calculated according to previous studies using the
690 following equation ^{65,66}:

691
$$\text{Relative fitness (r)} = \frac{X_1(1 - X_0)}{X_0(1 - X_1)}$$

692 X_0 : initial mutant frequency; $(1-X_0)$: initial ancestor frequency. X_1 : final mutant frequency; $(1-X_1)$:
693 final ancestor frequency.

694

695 **References and Notes:**

- 696 1. Berendsen, R. L., Pieterse, C. M. J. & Bakker, P. A. H. M. The rhizosphere microbiome
697 and plant health. *Trends Plant Sci.* **17**, 478–486 (2012).
- 698 2. Philippot, L., Raaijmakers, J. M., Lemanceau, P. & van der Putten, W. H. Going back to
699 the roots: the microbial ecology of the rhizosphere. *Nat. Rev. Microbiol.* **11**, 789–799
700 (2013).
- 701 3. Dethlefsen, L., McFall-Ngai, M. & Relman, D. A. An ecological and evolutionary
702 perspective on human–microbe mutualism and disease. *Nature* **449**, 811–818 (2007).
- 703 4. Brownlie, J. C. & Johnson, K. N. Symbiont-mediated protection in insect hosts. *Trends*
704 *Microbiol.* **17**, 348–354 (2009).
- 705 5. Kiers, E. T. & Denison, R. F. Sanctions, cooperation, and the stability of plant-rhizosphere
706 mutualisms. *Annu. Rev. Ecol. Evol. Syst.* **39**, 215–236 (2008).
- 707 6. King, K. C. *et al.* Rapid evolution of microbe-mediated protection against pathogens in a
708 worm host. *ISME J.* **10**, 1915–1924 (2016).
- 709 7. Tso, G. H. W. *et al.* Experimental evolution of a fungal pathogen into a gut symbiont.
710 *Science* **362**, 589–595 (2018).
- 711 8. Berendsen, R. L. *et al.* Disease-induced assemblage of a plant-beneficial bacterial
712 consortium. *ISME J.* **12**, 1496–1507 (2018).
- 713 9. Sasse, J., Martinoia, E. & Northen, T. Feed your friends: do plant exudates shape the root
714 microbiome? *Trends Plant Sci.* **23**, 25–41 (2018).
- 715 10. Bakker, P. A. H. M., Pieterse, C. M. J., de Jonge, R. & Berendsen, R. L. The soil-borne
716 legacy. *Cell* **172**, 1178–1180 (2018).
- 717 11. Johnson, N. C., Graham, J. H. & Smith, F. A. Functioning of mycorrhizal associations
718 along the mutualism-parasitism continuum. *New Phytol.* **135**, 575–586 (1997).
- 719 12. Kogel, K. H., Franken, P. & Hückelhoven, R. Endophyte or parasite - what decides? *Curr.*
720 *Opin. Plant Biol.* **9**, 358–363 (2006).
- 721 13. Cosme, M., Fernández, I., Van der Heijden, M. G. A. & Pieterse, C. M. J. Non-
722 mycorrhizal plants: the exceptions that prove the rule. *Trends in Plant Science* **23**, 577–
723 587 (2018).
- 724 14. Wein, T. *et al.* Currency, exchange, and inheritance in the evolution of symbiosis. *Trends*
725 *Microbiol.* **27**, 836–849 (2019).
- 726 15. Chomicki, G., Kiers, E. T. & Renner, S. S. The evolution of mutualistic dependence. *Annu.*
727 *Rev. Ecol. Evol. Syst.* **51**, annurev-ecolsys-110218-024629 (2020).
- 728 16. Stringlis, I. A., Zhang, H., Pieterse, C. M. J., Bolton, M. D. & De Jonge, R. Microbial
729 small molecules-weapons of plant subversion. *Natural Product Reports* **35**, 410–433
730 (2018).
- 731 17. Kramer, J., Özkaya, Ö. & Kümmerli, R. Bacterial siderophores in community and host
732 interactions. *Nature Reviews Microbiology* **18**, 152–163 (2020).
- 733 18. Kawecki, T. J. *et al.* Experimental evolution. *Trends Ecol. Evol.* **27**, 547–560 (2012).
- 734 19. Jousset, A., Lara, E., Wall, L. G. & Valverde, C. Secondary metabolites help biocontrol
735 strain *Pseudomonas fluorescens* CHA0 to escape protozoan grazing. *Appl. Environ.*
736 *Microbiol.* **72**, 7083–7090 (2006).
- 737 20. Brazelton, J. N., Pfeufer, E. E., Sweat, T. A., Gardener, B. B. M. & Coenen, C. 2, 4-
738 Diacetylphloroglucinol alters plant root development. *Mol. Plant-Microbe Interact.* **21**,
739 1349–1358 (2008).
- 740 21. Chaparro, J. M. *et al.* Root exudation of phytochemicals in *Arabidopsis* follows specific
741 patterns that are developmentally programmed and correlate with soil microbial functions.

- 742 *PLoS One* **8**, e55731 (2013).
- 743 22. Stringlis, I. A. *et al.* MYB72-dependent coumarin exudation shapes root microbiome
744 assembly to promote plant health. *Proc. Natl. Acad. Sci. U. S. A.* **115**, E5213–E5222
745 (2018).
- 746 23. Voges, M. J. E. E., Bai, Y., Schulze-Lefert, P. & Sattely, E. S. Plant-derived coumarins
747 shape the composition of an *Arabidopsis* synthetic root microbiome. *Proc. Natl. Acad. Sci.*
748 *U. S. A.* **116**, 12558–12565 (2019).
- 749 24. Zamioudis, C. *et al.* Rhizobacterial volatiles and photosynthesis-related signals coordinate
750 *MYB72* expression in *Arabidopsis* roots during onset of induced systemic resistance and
751 iron-deficiency responses. *Plant J.* **84**, 309–322 (2015).
- 752 25. Barrick, J. E. & Lenski, R. E. Genome dynamics during experimental evolution. *Nat. Rev.*
753 *Genet.* **14**, 827–839 (2013).
- 754 26. Yang, L. *et al.* Evolutionary dynamics of bacteria in a human host environment. *Proc.*
755 *Natl. Acad. Sci.* **108**, 7481–7486 (2011).
- 756 27. Haas, D. & Défago, G. Biological control of soil-borne pathogens by fluorescent
757 pseudomonads. *Nat. Rev. Microbiol.* **3**, 307–319 (2005).
- 758 28. Reyrat, J. M., David, M., Batut, J. & Boistard, P. FixL of *Rhizobium meliloti* enhances the
759 transcriptional activity of a mutant FixJD54N protein by phosphorylation of an alternate
760 residue. *J. Bacteriol.* **176**, 1969–1976 (1994).
- 761 29. Laville, J. *et al.* Global control in *Pseudomonas fluorescens* mediating antibiotic synthesis
762 and suppression of black root rot of tobacco. *Proc. Natl. Acad. Sci.* **89**, 1562–1566 (1992).
- 763 30. Bull, C. T. *et al.* Characterization of spontaneous *gacS* and *gacA* regulatory mutants of
764 *Pseudomonas fluorescens* biocontrol strain CHA0. *Antonie Van Leeuwenhoek* **79**, 327–336
765 (2001).
- 766 31. Zhang, R. *et al.* Structure of a bacterial quorum-sensing transcription factor complexed
767 with pheromone and DNA. *Nature* **417**, 971–974 (2002).
- 768 32. Battesti, A., Majdalani, N. & Gottesman, S. The RpoS-mediated general stress response in
769 *Escherichia coli*. *Annu. Rev. Microbiol.* **65**, 189–213 (2011).
- 770 33. Stockwell, V. O. & Loper, J. E. The sigma factor RpoS is required for stress tolerance and
771 environmental fitness of *Pseudomonas fluorescens* Pf-5. *Microbiology* **151**, 3001–3009
772 (2005).
- 773 34. Heeb, S., Valverde, C. & Haas, D. Role of the stress sigma factor RpoS in GacA / RsmA-
774 controlled secondary metabolism and resistance to oxidative stress in *Pseudomonas*
775 *fluorescens* CHA0. *FEMS Microbiol. Lett.* **243**, 251–258 (2005).
- 776 35. Whiteley, M. *et al.* Gene expression in *Pseudomonas aeruginosa* biofilms. *Nature* **413**,
777 860–864 (2001).
- 778 36. Ramey, B. E., Koutsoudis, M., Bodman, S. B. V. & Fuqua, C. Biofilm formation in plant-
779 microbe associations. *Current Opinion in Microbiology* **7**, 602–609 (2004).
- 780 37. Fukami, T., Beaumont, H. J. E., Zhang, X. X. & Rainey, P. B. Immigration history
781 controls diversification in experimental adaptive radiation. *Nature* **446**, 436–439 (2007).
- 782 38. Fukami, T. Historical contingency in community assembly: integrating niches, species
783 pools, and priority effects. *Annu. Rev. Ecol. Evol. Syst.* **46**, 1–23 (2015).
- 784 39. Rainey, P. B. & Travisano, M. Adaptive radiation in a heterogeneous environment. *Nature*
785 **394**, 69–70 (1998).
- 786 40. Gómez, P. & Buckling, A. Real-time microbial adaptive diversification in soil. *Ecol. Lett.*
787 **16**, 650–655 (2013).
- 788 41. Houte, S. *et al.* Compost spatial heterogeneity promotes evolutionary diversification of a

- 789 bacterium. *J. Evol. Biol.* jeb.13722 (2020). doi:10.1111/jeb.13722
- 790 42. Klironomos, J. N. Feedback with soil biota contributes to plant rarity and invasiveness in
791 communities. *Nature* **417**, 67–70 (2002).
- 792 43. Kardol, P., Martijn Bezemer, T. & van der Putten, W. H. Temporal variation in plant-soil
793 feedback controls succession. *Ecol. Lett.* **9**, 1080–1088 (2006).
- 794 44. Batstone, R. T., O’Brien, A. M., Harrison, T. L. & Frederickson, M. E. Experimental
795 evolution makes microbes more cooperative with their local host genotype. *Science* **370**,
796 476–478 (2020).
- 797 45. Ramette, A. *et al.* *Pseudomonas protegens* sp. nov., widespread plant-protecting bacteria
798 producing the biocontrol compounds 2,4-diacetylphloroglucinol and pyoluteorin. *Syst.*
799 *Appl. Microbiol.* **34**, 180–188 (2011).
- 800 46. Stutz, E. W., Défago, G. & Kern, H. Naturally occurring fluorescent pseudomonads
801 involved in suppression of black root rot of tobacco. *Phytopathology* **76**, 181–185 (1986).
- 802 47. Jousset, A. *et al.* Full-genome sequence of the plant growth-promoting bacterium
803 *Pseudomonas protegens* CHA0. *Genome Announc.* **2**, e00322-14 (2014).
- 804 48. King, E. O., Ward, M. K. & Raney, D. E. Two simple media for the demonstration of
805 pyocyanin and fluorescein. *J. Lab. Clin. Med.* **44**, 301–307 (1954).
- 806 49. Glickmann, E. & Dessaux, Y. A critical examination of the specificity of the salkowski
807 reagent for indolic compounds produced by phytopathogenic bacteria. *Appl. Environ.*
808 *Microbiol.* **61**, 793–796 (1995).
- 809 50. Alexander, D. B. & Zuberer, D. A. Use of chrome azurol S reagents to evaluate
810 siderophore production by rhizosphere bacteria. *Biol. Fertil. Soils* **12**, 39–45 (1991).
- 811 51. Smeltzer, M. S., Hart, M. E. & Iandolo, J. J. Phenotypic characterization of *xpr*, a global
812 regulator of extracellular virulence factors in *Staphylococcus aureus*. *Infect. Immun.* **61**,
813 919–925 (1993).
- 814 52. Oberhänsli, T., Défago, G. & Haas, D. Indole-3-acetic acid (IAA) synthesis in the
815 biocontrol strain CHA0 of *Pseudomonas fluorescens*: role of tryptophan side chain
816 oxidase. *Microbiology* **137**, 2273–2279 (1991).
- 817 53. Moskowitz, S. M., Foster, J. M., Emerson, J. & Burns, J. L. Clinically feasible biofilm
818 susceptibility assay for isolates of *Pseudomonas aeruginosa* from patients with cystic
819 fibrosis. *J. Clin. Microbiol.* **42**, 1915–1922 (2004).
- 820 54. Harrison, J. J. *et al.* Microtiter susceptibility testing of microbes growing on peg lids: a
821 miniaturized biofilm model for high-throughput screening. *Nat. Protoc.* **5**, 1236–1254
822 (2010).
- 823 55. Zamioudis, C., Mastranesti, P., Dhonukshe, P., Blilou, I. & Pieterse, C. M. J. Unraveling
824 root developmental programs initiated by beneficial *Pseudomonas* spp bacteria. *Plant*
825 *Physiol.* **162**, 304–318 (2013).
- 826 56. Højberg, O., Schnider, U., Winteler, H. V., Sørensen, J. & Haas, D. Oxygen-sensing
827 reporter strain of *Pseudomonas fluorescens* for monitoring the distribution of low-oxygen
828 habitats in soil. *Appl. Environ. Microbiol.* **65**, 4085–4093 (1999).
- 829 57. Millet, Y. A. *et al.* Innate immune responses activated in *Arabidopsis* roots by microbe-
830 associated molecular patterns. *Plant Cell* **22**, 973–990 (2010).
- 831 58. Hafner, M., Niepel, M., Chung, M. & Sorger, P. K. Growth rate inhibition metrics correct
832 for confounders in measuring sensitivity to cancer drugs. *Nat. Methods* **13**, 521–527
833 (2016).
- 834 59. Tritt, A., Eisen, J. A., Facciotti, M. T. & Darling, A. E. An integrated pipeline for de novo
835 assembly of microbial genomes. *PLoS One* **7**, e42304 (2012).

- 836 60. Seemann, T. Prokka: rapid prokaryotic genome annotation. *Bioinformatics* **30**, 2068–2069
837 (2014).
- 838 61. Quinlan, A. R. & Hall, I. M. BEDTools: a flexible suite of utilities for comparing genomic
839 features. *Bioinformatics* **26**, 841–842 (2010).
- 840 62. Kai Lee, H. *et al.* High-resolution melting approach to efficient identification and
841 quantification of H275Y mutant influenza H1N1/2009 virus in mixed-virus-population
842 samples. *J. Clin. Microbiol.* **49**, 3555–3559 (2011).
- 843 63. Zhong, W.-L. *et al.* Development of unlabeled probe based high-resolution melting
844 analysis for detection of filaggrin gene mutation c.3321delA. *J. Clin. Lab. Anal.* **30**, 892–
845 896 (2016).
- 846 64. Capper, R. L. *et al.* Quantitative high resolution melting: two methods to determine SNP
847 allele frequencies from pooled samples. *BMC Genet.* **16**, 62 (2015).
- 848 65. Jousset, A. *et al.* Predators promote defence of rhizosphere bacterial populations by
849 selective feeding on non-toxic cheaters. *ISME J.* **3**, 666–674 (2009).
- 850 66. Ross-Gillespie, A., Gardner, A., West, S. A. & Griffin, A. S. Frequency dependence and
851 cooperation: theory and a test with bacteria. *Am. Nat.* **170**, 331–342 (2007).
852

853 **Acknowledgments:**

854 We thank Roy van der Meijs for his excellent work on the scopoletin sensitivity assays and Ke Yu,
855 Roeland Berendsen and members of the Plant-Microbe Interactions lab for helpful discussion. This
856 work was supported by a China Scholarship Council fellowship (to E.L.), a postdoctoral fellowship
857 of the Research Foundation Flanders (FWO 12B8116RN) (to R.D.J.) and Royal Society Research
858 Grants (grant nos. RSG\R1\180213 and CHL\R1\180031) at the University of York (V-P.F).

859 **Author contributions:**

860 EL, PB and AJ designed the experiments. EL, HJ and CL performed the experiment. EL, RJ and
861 AJ analysed the data. All authors collegially wrote the manuscript.

862 **Declaration of Interests:**

863 Authors declare no competing interests.

864

865 **Supplementary Materials for**

866 **Rapid evolution of bacterial mutualism in the plant rhizosphere**

867 **Data and materials availability:**

868 The *P. protegens* CHA0-GFP reference strain genome sequence, determined for this study, is
869 deposited on GenBank: [RCSR00000000.1](#). Raw sequencing data used in this study are deposited
870 at the NCBI database under BioProject [PRJNA473919](#). Raw data of *P. protegens* CHA0
871 phenotypic traits, Supplementary dataset 1 and 2, are deposited at Mendeley Data: DOI:
872 [10.17632/wh3ytm5rn8.1](#)

873

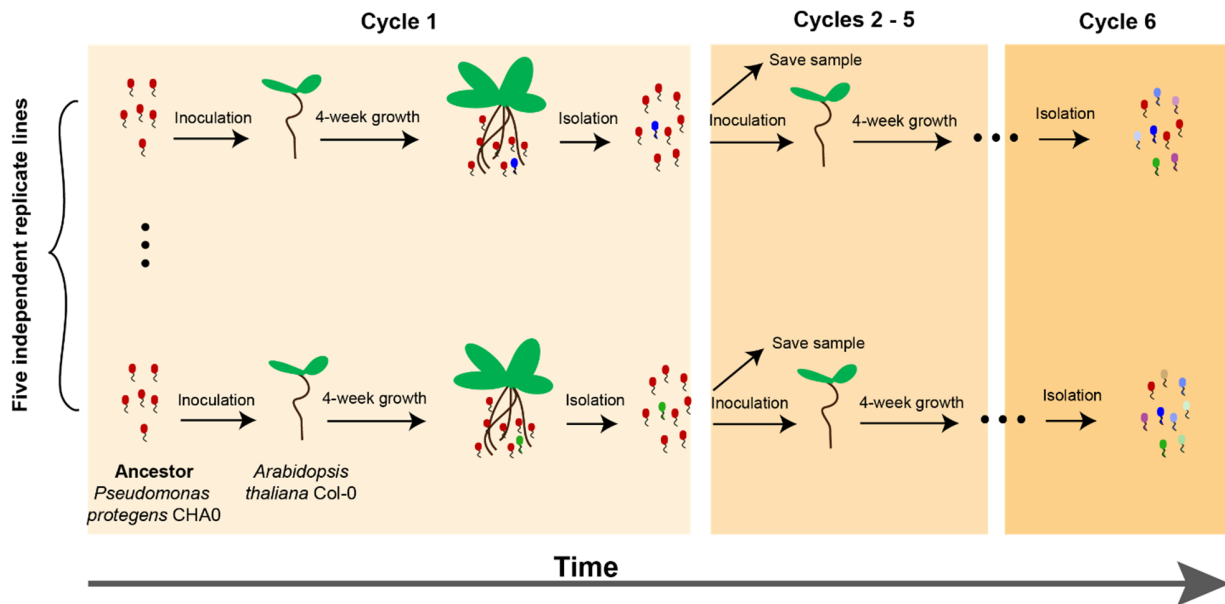
874 **The following file includes:**

875 Figs. S1 to S7

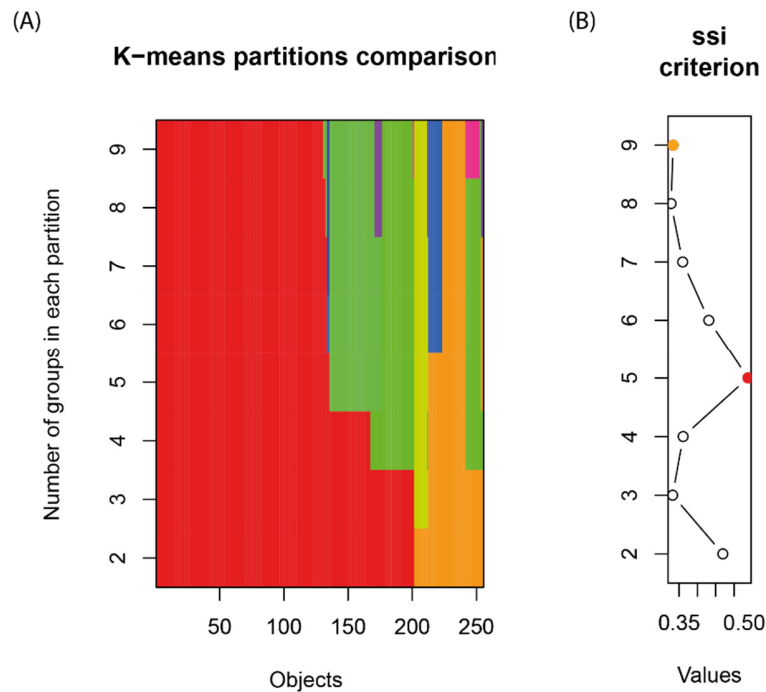
876 Tables S1 to S4

877 Legends of supplementary dataset 1 and 2

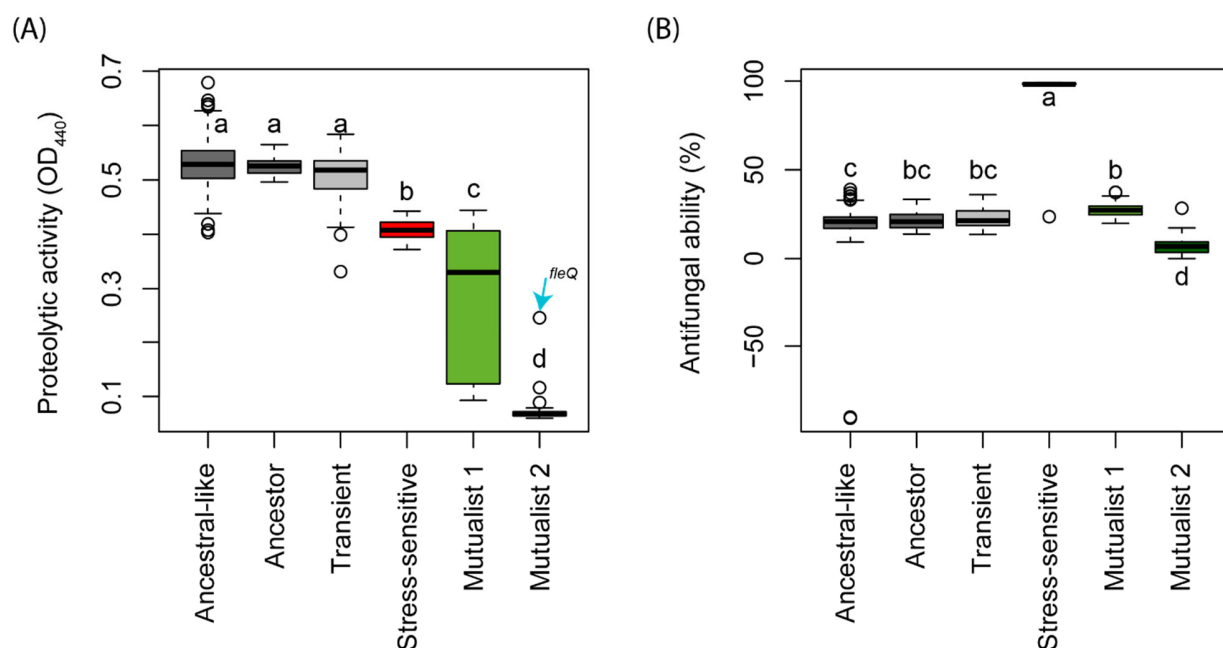
878 **Supplementary figures:**



879
880 **Figure S1. Overview of the experimental design.** In this study, we experimentally evolved
881 *Pseudomonas protegens* CHA0 in the rhizosphere of sterile *Arabidopsis thaliana* plants. We used
882 a gnotobiotic, organic carbon-free soil system in which bacterial fitness strictly depended on their
883 interaction with plants. We set up five independent plant replicate lines, which were passed over
884 six plant growth cycles (4 weeks each). To this end, 10^6 cells of the ancestral *P. protegens* CHA0
885 strain were introduced to the rhizosphere of two *A. thaliana* seedlings grown in sterile silver sand
886 supplemented with a plant nutrient solution in sterile ECO2 boxes. At the end of each growth cycle,
887 the rhizosphere bacterial population was harvested, and 10^6 cells were inoculated onto a new plant.
888 The remaining bacteria were kept as frozen stock at $-80\text{ }^{\circ}\text{C}$. At the end of the experiment, bacteria
889 from the $-80\text{ }^{\circ}\text{C}$ stock were plated on 3 g l^{-1} Tryptic Soy Agar and sixteen single bacterial isolates
890 were randomly selected from each replicate line at the end of the second, fourth and sixth growth
891 cycle. In total, 240 evolved isolates and sixteen ancestral isolates were phenotyped regarding traits
892 associated with bacterial fitness and mutualistic activity with the plant.

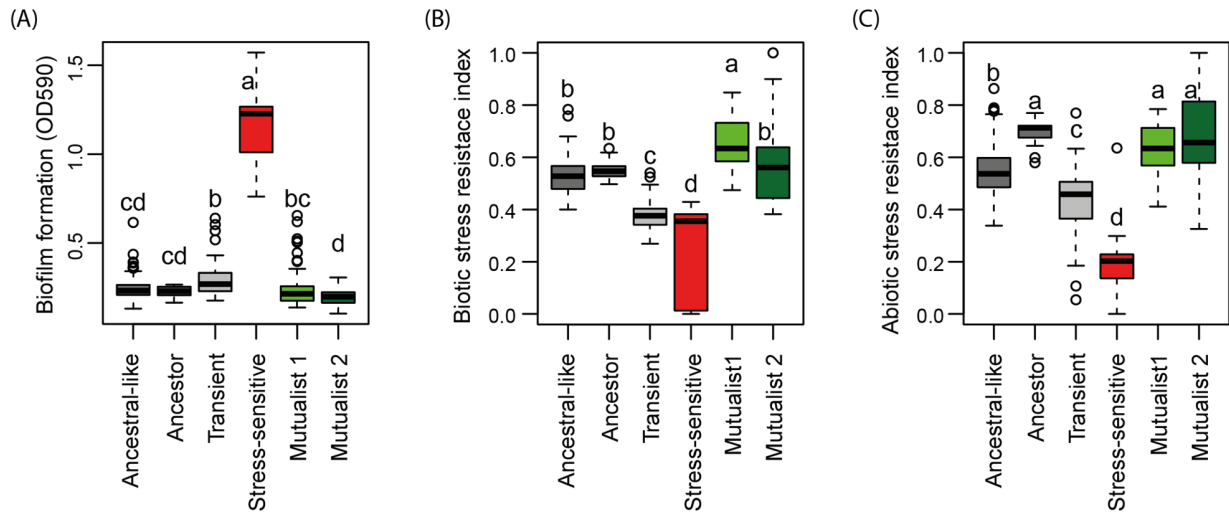


893
894 **Figure S2. K-means clustering analysis of evolved *Pseudomonas protegens* CHA0 isolates.**
895 Isolated colonies were classified based on 14 phenotypic traits associated with bacterial fitness in
896 the rhizosphere and mutualistic activity with the plant. In panel A, the x-axis (“Objects”) represents
897 the 256 screened isolates while the y-axis represents the potential number of clusters (K) shown in
898 different colours. Panel B shows the SSI criterion values indicating the most parsimonious number
899 of clusters needed to classify isolates into distinct phenotypic groups. Based on this analysis, we
900 classified the isolates into five clusters (the highest SSI criterion value).



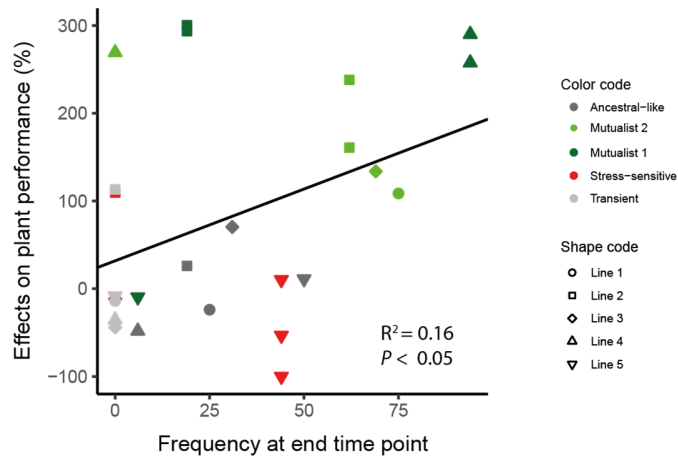
901
902 **Figure S3. Comparing the differences in extracellular proteolytic and antifungal activity of**
903 **ancestral and evolved *Pseudomonas protegens* CHA0 isolates.** We measured the proteolytic (A)
904 and antifungal activity (B) as a proxy for secondary metabolite production. In total, we
905 characterized 16 ancestral, 119 ancestral-like, 11 stress-sensitive, 37 mutualist 1, 31 mutualist 2
906 and 41 transient isolates (Supplementary dataset 1). In panel A, the blue arrow indicates one isolate
907 that was phenotypically clustered as mutualist 2, but genetically bearing a unique *fleQ* mutation.
908 Statistical testing was carried out using ANOVA. Different letters indicate significant differences
909 based on a Tukey HSD test ($\alpha=0.05$).

910

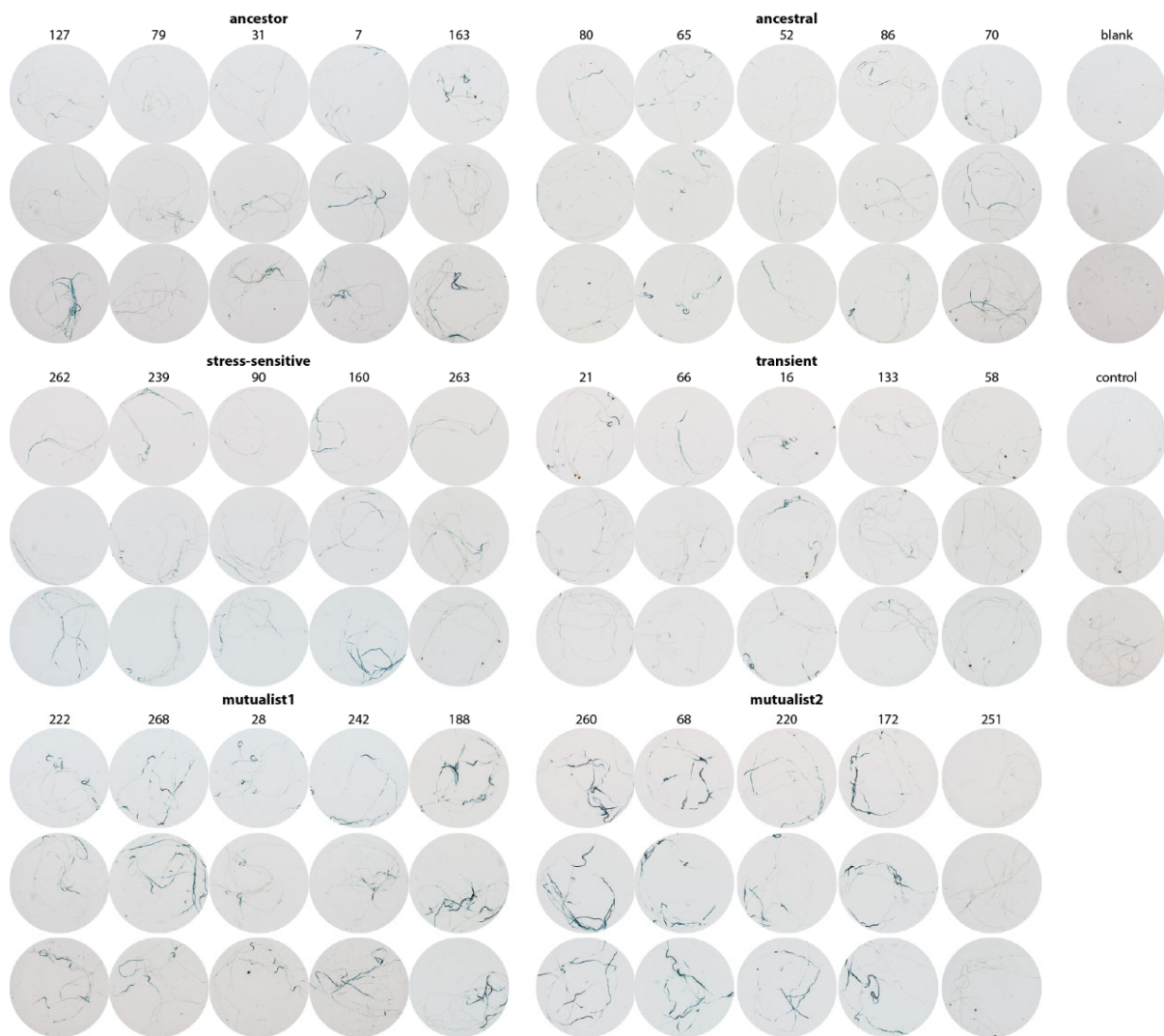


911

912 **Figure S4. Comparing biofilm formation, biotic and abiotic stress resistance of ancestral and**
913 **evolved *Pseudomonas protegens* CHA0 isolates.** In total, we characterized 16 ancestral, 119
914 ancestral-like, 11 stress-sensitive, 37 mutualist 1, 31 mutualist 2 and 41 transient isolates
915 (Supplementary dataset 1). Panels A to C show biofilm formation, biotic stress resistance index
916 (normalised PC1 of combined ability to grow in the presence of sub lethal doses of the antibiotics
917 streptomycin, tetracycline and penicillin) and abiotic stress resistance index (normalised first
918 principal component of combined ability of each isolate to grow under oxidative stress, water
919 potential stress and salt stress) respectively. Statistical testing was carried out using ANOVA.
920 Different letters indicate significant differences based on a Tukey HSD test ($\alpha=0.05$).



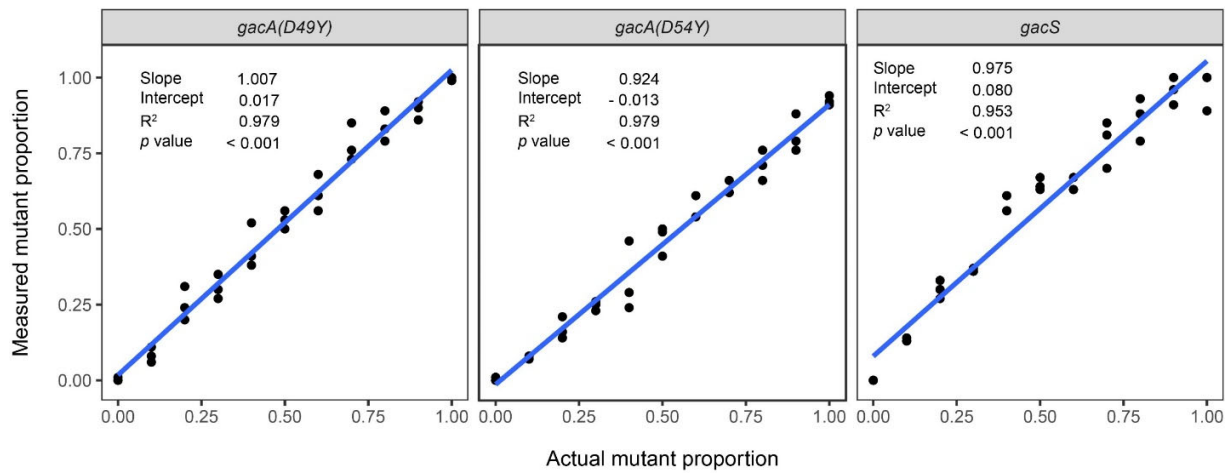
921
922
923 **Figure S5. Positive relationship between phenotype frequency at the end of the selection**
924 **experiment and isolate effect on the plant performance.** Five representative bacterial isolates
925 from each phenotype in addition to the ancestor were selected to measure their effects on
926 *Arabidopsis thaliana* growth in terms of combined ‘Plant performance’ index (30 isolates
927 altogether, each replicate line represented; See Table S2). The y-axis represents the beneficial
928 effect of isolates on plant performance relative to the ancestor. Values on the x-axis show the
929 relative abundance of evolved phenotypes in their respective selection lines at the end of the sixth
930 plant growth cycle (see Figure 1). Colours and shapes represent different phenotypes and selection
931 lines, respectively.



932

933

934 **Figure S6. Induction of MYB72 assayed in a GUS reporter line in *Arabidopsis thaliana* by the**
935 **ancestor and a subset of evolved *Pseudomonas protegens* CHA0 isolates.** GUS staining was
936 performed at 2 days after bacterial inoculation (n = 3 biological plant replicates, each containing 5
937 to 6 seedlings). See Table S2 for detailed information of the isolates.



938
939 **Figure S7** Standard curves of measured mutant versus ancestor proportion as a function of the
940 actual proportion, using series of mixed samples with known proportions (0%, 10%, 20%, 30%,
941 40%, 50%, 60%, 70%, 80%, 90% and 100% of mutant templates). Relative densities of mutant
942 *gacA*^{D49Y}, *gacA*^{D54Y}, and *gacS*^{G27D} were measured by PCR-based high-resolution melting profile
943 (RQ-HRM) analysis. Measurements for each sample were done in triplicate. In each plot, the black
944 dots represent the measurements, the blue fit line was generated based on linear regression model.
945

946 **Table S1.** *In vitro* measurement of different aspects of bacterial life-history traits, including
 947 bacterial growth, tolerance to diverse abiotic and biotic stresses, production (or activity) of
 948 bioactive compounds and antimicrobial activity. In total, 14 different phenotypic traits were
 949 measured for 256 *Pseudomonas protegens* CHA0 isolates in this study including 16 isolated
 950 isolates of ancestor.

Aspects of life-history traits	Details of measured traits
Bacterial growth yield	Bacterial growth yield in King's medium B
Stress tolerance	Growth yield under abiotic stresses: oxidative stress, water potential stress, salt stress Growth yield under biotic stresses (antibiotics): streptomycin stress, tetracycline stress, penicillin stress
Production (or activity) of bioactive compounds	IAA (auxin) production, siderophore activity, quorum sensing (TSO) activity, proteolytic activity, biofilm formation
Antimicrobial activity	Antifungal activity: <i>Verticillium dahliae</i> Antibacterial activity: <i>Ralstonia solanacearum</i>

951

952 **Table S2.** Description of 5 ancestral and 25 evolved *Pseudomonas protegens* CHA0 isolates, which
 953 were included to phenotyping and genotyping assays. “Sample ID” is the unique identifier of each
 954 isolate and five isolates were selected from each phenotype class. The “Plant cycle” column refers
 955 to the plant growth cycle from which the isolate was collected (see Figure S1) and the “Replicate”
 956 column refers to the independent plant replicate selection line. Mutated genes were identified using
 957 whole genome re-sequencing. On average, each evolved isolate encompassed 2-3 mutations
 958 relative to the ancestral sequence that are typically non-synonymous in nature, *i.e.* they directly
 959 affect predicted protein sequence and/or protein length. The same Sample ID superscript numbers
 960 shown on bold (133 and 242, 66 and 222, 28 and 220) indicate paired samples used in relative
 961 competition assays presented in Figure 5.
 962

Phenotype	Sample ID	Plant cycle	Replicate	Genotype
Ancestor	7	0	Ancestor	—
Ancestor	31	0	Ancestor	—
Ancestor	79	0	Ancestor	—
Ancestor	127	0	Ancestor	—
Ancestor	163	0	Ancestor	—
Ancestral-like	52	4	Line 2	<i>galE</i> ^{V32M}
Ancestral-like	65	2	Line 3	—
Ancestral-like	70	4	Line 5	—
Ancestral-like	80	4	Line 4	—
Ancestral-like	86	4	Line 1	<i>oafA</i> ^{Y335X} · <i>RS17350</i> ^{A77A.fsX14} · <i>wbpM</i> ^{G79R}
Stress-sensitive	90	4	Line 3	<i>nlpD</i> ^{Q197P}
Stress-sensitive	160	4	Line 2	<i>galE</i> ^{V32M} · <i>accC</i> ^{E413K} · <i>yvaQ2</i> ^{-9G>T}
Stress-sensitive	239	6	Line 5	<i>rpoS</i> ^{Q65X} · <i>tetR</i> ^{Y127X}
Stress-sensitive	262	6	Line 5	<i>rpoS</i> ^{Q65X}
Stress-sensitive	263	6	Line 5	<i>rpoS</i> ^{Q65X}
Mutualist 1	28²	4	Line 2	<i>galE</i> ^{V32M} · <i>accC</i> ^{E413K}
Mutualist 1	188	4	Line 4	<i>gacA</i> ^{-40T>A}
Mutualist 1	222³	6	Line 3	<i>oafA</i> ^{K338S.fsX18} · <i>gacS</i> ^{G27D}

Mutualist 1	242¹	6	Line 1	<i>oafA</i> ^{Y335X} . <i>RS17350</i> ^{A77A.fsX14} . <i>gacA</i> ^{D49Y}
Mutualist 1	268	6	Line 2	<i>galE</i> ^{V32M} . <i>accC</i> ^{E413K} . <i>gacA</i> ^{G97S} . <i>mraZ</i> ^{211A>G}
Mutualist 2	68	4	Line 4	<i>gacA</i> ^{-40T>A} . <i>RS11820</i> ^{33C>T}
Mutualist 2	172	4	Line 2	<i>gacA</i> ^{Y183S}
Mutualist 2	220²	6	Line 2	<i>galE</i> ^{V32M} . <i>accC</i> ^{E413K} . <i>gacA</i> ^{D54Y}
Mutualist 2	251	6	Line 5	<i>fleQ</i> ^{R320Q}
Mutualist 2	260	6	Line 4	<i>gacA</i> ^{E38X} . <i>RS11785</i> ^{S256C} . <i>flhA</i> ^{H393Q.fsX15}
Transient	16	4	Line 2	<i>galE</i> ^{V32M} . <i>accC</i> ^{E413K}
Transient	21	2	Line 4	<i>hult</i> ^{786C>T}
Transient	58	4	Line 5	–
Transient	66³	4	Line 3	<i>oafA</i> ^{K338S.fsX18}
Transient	133¹	2	Line 1	<i>oafA</i> ^{Y335X} . <i>RS17350</i> ^{A77A.fsX14}

963

964 Note: X, represents a stop codon (at its relative position in case of a shifted frame); fs, frame shift; sequence
965 change positions are relative to the cDNA.

966 **Table S3.** Overview of the affected genes that are identified in the 25 evolved *Pseudomonas protegens* CHA0 isolates (See Table S2).

<i>Gene</i>	<i>Product</i>	<i>Locus tag</i>	<i>DNA change</i>	<i>Effect</i>
<i>accC</i>	Biotin carboxylase, acetyl-CoA carboxylase	PFLCHA0_RS03400	c.1237 G>A	p.E413K
<i>flhA</i>	Flagellar biosynthesis protein FlhA	PFLCHA0_RS08490	c.1154 T deleted	early stop
<i>gacA</i>	Response regulator GacA	PFLCHA0_RS17965	c.548 A>C	p.Y183S
<i>gacA</i>	Response regulator GacA	PFLCHA0_RS17965	c.289 G>A	p.G97S
<i>gacA</i>	Response regulator GacA	PFLCHA0_RS17965	c.160 G>T	p.D54Y
<i>gacA</i>	Response regulator GacA	PFLCHA0_RS17965	c.145 G>T	p.D49Y
<i>gacA</i>	Response regulator GacA	PFLCHA0_RS17965	c.112 G>T	p.E38*
<i>gacA</i>	Response regulator GacA	PFLCHA0_RS17965	-40 T>A	promoter
<i>galE</i>	UDP-glucose 4-epimerase	PFLCHA0_RS09920	c.94 G>A	p.V32M
<i>RS11785</i>	LysR family transcriptional regulator	PFLCHA0_RS11785	c.766 A>T	p.S256C
<i>hutI</i>	Imidazolonepropionase	PFLCHA0_RS02080	c.786 C>T	synonymous
<i>RS11820</i>	PaaI family thioesterase	PFLCHA0_RS11820	c.33 C>T	synonymous
<i>yvaQ2</i>	Methyl-accepting chemotaxis protein	PFLCHA0_RS13000	-9bp G>T	promoter
<i>mraZ</i>	Transcriptional regulator mraZ	PFLCHA0_RS25175	-211bp A>G	promoter
<i>nlpD</i>	Lipoprotein nlpD/lppB/LysM domain-containing protein	PFLCHA0_RS31060	c.590 A>C	p.Q197P
<i>fleQ</i>	Sigma-54-dependent Fis family transcriptional regulator	PFLCHA0_RS08340	c.959 G>A	p.R320Q
<i>oafA</i>	O-acetyltransferase OatA	PFLCHA0_RS09890	c.1005 C>A	p.Y335*
<i>oafA</i>	O-acetyltransferase OatA	PFLCHA0_RS09890	c.1009 A deleted	early stop

<i>wbpM</i>	Polysaccharide biosynthesis protein/NDP-sugar epimerase	PFLCHA0_RS21855	c.235 G>C	p.G79R
<i>rpoS</i>	RNA polymerase sigma factor RpoS	PFLCHA0_RS06125	c.193 C>T	p.Q65*
<i>RS17350</i>	Methyltransferase domain-containing protein	PFLCHA0_RS17350	c.116 C deleted	early stop

967

968 **Table S4** Primers and probes used for high-resolution melting (HRM) analysis. For the two *gacA* mutants the same set of primers was
 969 used. Underlined bases indicate the position of the single nucleotide point (SNP) mutations within the probe sequences. ΔT_m ($^{\circ}\text{C}$)
 970 indicates the melting temperature difference between WT-probe duplex and mutant-probe duplex.

Target gene	Strain ID	SNP locus	Forward primer (excess)	Reverse primer (limiting)	Amplicon size	Probe sequence	Probe length	Target strand	Perfect match/mismatch	ΔT_m ($^{\circ}\text{C}$)
<i>gacA</i> ^{D49Y}	242	145G>T	5'- ATCGATGGCCTGCAAGTAG T-3'	5'- CGGGTAGGAAAGGGATCTTC- 3'	206 bp	5'- CATCAGGACCACA <u>T</u> CGGGCTTCAGCT CCCG-/C3/3'	30nt	WT	G::C / T::C	5.31
<i>gacA</i> ^{D54Y}	220	160G>T	5'- ATCGATGGCCTGCAAGTAG T-3'	5'- CGGGTAGGAAAGGGATCTTC- 3'	206 bp	5'- TGGCATCTTGACG <u>T</u> CATCAGGACCA CATC-/C3/3'	30nt	WT	G::C / T::C	4.92
<i>gacS</i> ^{G27D}	222	80G>A	5'- GCGTACTGTTGCTGACCTTG -3'	5'- AGCATCTGGGTGTTGTGGTT- 3'	178bp	5'- AGGTGAAGTAGCC <u>G</u> CCAGCACCAA GCCA-/C3/3'	30nt	WT	G::C / A::C	4.83

971

972 **Supplementary dataset 1:** Sheet 1: Summary table for the set of fourteen phenotypic traits for the 256 characterised isolates used for
973 K-mean clustering. Sheet 2: Carbon use data for the 256 characterised isolates. In both sheets, each line corresponds to one isolate and
974 each column to one specific trait. See material and methods for a detailed description of experimental procedures.

975 **Supplementary dataset 2:** Sheet 1: Recapitulation of the origin (replicate line), time point and phenotype of each of the 30 isolates
976 tested in details for their interactions with the host plant. Sheet 2: Summary table for interactions between each of the 30 isolates tested
977 for plant growth, including effect on plant performance and induced GUS expression. Sheet 3: Scopoletin sensitivity. See material and
978 methods for a detailed description of experimental procedures.